

PHILOS. TRANS. R. SOC. A

rspa.royalsocietypublishing.org

Article submitted to journal

**Subject Areas:**

Uranus; Neptune; Ice Giants;  
Planetary Atmospheres; Atmospheric  
Chemistry

**Keywords:**

Uranus; Neptune; Photochemistry;  
Atmospheric Chemistry; Planetary  
Atmospheres

**Author for correspondence:**

Julianne I. Moses  
e-mail: [jmoses@spacescience.org](mailto:jmoses@spacescience.org)

## Atmospheric chemistry on Uranus and Neptune

J. I. Moses<sup>1</sup>, T. Cavalié<sup>2,3</sup>, L. N. Fletcher<sup>4</sup>,  
and M. T. Roman<sup>4</sup>

<sup>1</sup>Space Science Institute, 4765 Walnut St., Suite B,  
Boulder, CO 80301, USA

<sup>2</sup>Laboratoire d'Astrophysique de Bordeaux, University  
of Bordeaux, CNRS, B18N, allée Geoffroy  
Saint-Hilaire, 33615 Pessac, France

<sup>3</sup>LESIA, Observatoire de Paris, 92195 Meudon, France

<sup>4</sup>University of Leicester, School of Physics and  
Astronomy, University Road, Leicester, LE1 7RH, UK

Comparatively little is known about atmospheric chemistry on Uranus and Neptune, because remote spectral observations of these cold, distant “Ice Giants” are challenging, and each planet has only been visited by a single spacecraft during brief flybys in the 1980s. Thermochemical equilibrium is expected to control the composition in the deeper, hotter regions of the atmosphere on both planets, but disequilibrium chemical processes such as transport-induced quenching and photochemistry alter the composition in the upper atmospheric regions that can be probed remotely. Surprising disparities in the abundance of disequilibrium chemical products between the two planets point to significant differences in atmospheric transport. The atmospheric composition of Uranus and Neptune can provide critical clues for unravelling details of planet formation and evolution, but only if it is fully understood how and why atmospheric constituents vary in a three-dimensional sense and how material coming in from outside the planet affects observed abundances. Future mission planning should take into account the key outstanding questions that remain unanswered about atmospheric chemistry on Uranus and Neptune, particularly those questions that pertain to planet formation and evolution, and those that address the complex, coupled atmospheric processes that operate on Ice Giants within our solar system and beyond.

## 1. Introduction

Uranus and Neptune have the dubious honor of being the least explored planets in our solar system. Even after the *Voyager 2* encounter with Uranus in 1986 and Neptune in 1989, many mysteries remain regarding the interior structure, atmospheric properties, and magnetic-field generation on these planets. It is also unclear how these Ice Giants formed. Traditional core-accretion planetary-formation models have difficulty getting the timing of Uranus and Neptune formation to work out correctly [1–3]. The main problem with these traditional models is that the planets tend to either grow too slowly to accrete much of the nebular gas in the protoplanetary disk before the gas is lost from the system, and so Uranus and Neptune end up as small solid planets without H<sub>2</sub>-He envelopes, or the planets grow so rapidly that they reach a runaway gas-accretion stage, and so they end up as H<sub>2</sub>-He dominated gas giants. Forming our Ice Giants with a substantial fraction of both heavy elements and H<sub>2</sub>-He requires precise timing and fine-tuning of the models. This difficulty has become exacerbated in the current exoplanet-discovery era, given that planets between the size of Earth and Neptune constitute a dominant fraction of the extrasolar planet population discovered to date [4–6]. We need to better understand how these volatile-rich, intermediate-sized planets form. The observable atmospheric composition of Uranus and Neptune — both from remote observations and future *in situ* probes — can provide important clues to formation location, formation mechanisms, protoplanetary disk conditions, and potential planetary migration history [7–9], thereby considerably advancing our knowledge of planet formation and evolution. However, the atmospheric composition of the Ice Giants can only provide these critical clues if we fully understand how various chemical processes are affecting the observed atmospheric composition, and how that observed composition relates to the bulk atmospheric composition.

Observations of atmospheric constituents on Uranus and Neptune also shed light on the complex physical and chemical processes currently operating within the atmospheres, thus addressing the important broad topic of “How planets work.” Chemistry controls the atmospheric composition, which in turn affects other aspects of the atmosphere, such as cloud and haze formation, thermal structure and radiative balance, and atmospheric dynamics and circulation. The three-dimensional distribution of atmospheric constituents — and its variation with time — reflect a complex coupling between atmospheric chemistry, dynamics, and energy transport in planetary atmospheres. Observations and models can help work out the details of this coupling. Some constituents may be good tracers for atmospheric dynamics, for example, but only if the sources, sinks, and overall chemistry of these species are well understood. The two broadly similar Ice Giants also provide a good launching point for comparative planetology. By studying the composition of both Uranus and Neptune, we can identify the physical and chemical characteristics that are responsible for their observed similarities and differences. The insight gained from this comparative-planetology approach may have relevance to studies of extrasolar planets.

In this paper, we review what is known and unknown about atmospheric chemistry on Uranus and Neptune. That chemistry has many similarities to Jupiter and Saturn. However, some differences arise among all our giant planets as a result of heavy-element content, atmospheric temperatures, atmospheric dynamics and circulation, and the stochastic nature of some processes, such as impacts, which can affect planetary obliquity, interior structure, interior mixing, internal heat flow, deep atmospheric convection, and atmospheric composition [10–14]. We will discuss the observed composition of Uranus and Neptune, as well as the key chemical processes that operate in various regions of the atmosphere, from the deep troposphere on up to the top of the atmosphere. Our *Voyager*-era understanding of atmospheric chemistry on Uranus and Neptune has been described in previous works [15–19]; here, we restrict our discussion to the major advances that have occurred since the mid-1990s.

## 2. Basic atmospheric properties and observed composition

The bulk composition of Uranus and Neptune by mass is roughly 10-20% hydrogen and helium and 80-90% heavier elements [20]. These heavier elements include refractory elements that traditionally form rocky materials and more volatile elements that traditionally form ices, but the relative proportions of “rock” and “ice” are unclear for both the planets as a whole, as well as for their atmospheres. What is clear is that the atmospheres themselves become progressively enriched with  $H_2$  and He with increasing altitude as elements condense out and are thereby removed from cooler higher-altitude regions, and then more significantly enriched in  $H_2$  and He at very high altitudes as mass separation occurs above the homopause. The atmospheres of Uranus and Neptune can be divided into three main regions: the *troposphere* in the lowest region, where convection occurs and temperatures are hot at depth and decrease with increasing altitude, the *stratosphere* or middle atmosphere above the tropopause temperature minimum, where radiative processes dominate and temperatures increase or are constant with increasing altitude, and the *thermosphere* in the uppermost regions of the atmosphere, where temperatures begin to increase more sharply as heat is conducted downward from a hot exosphere at high altitudes (see Fig. 1).

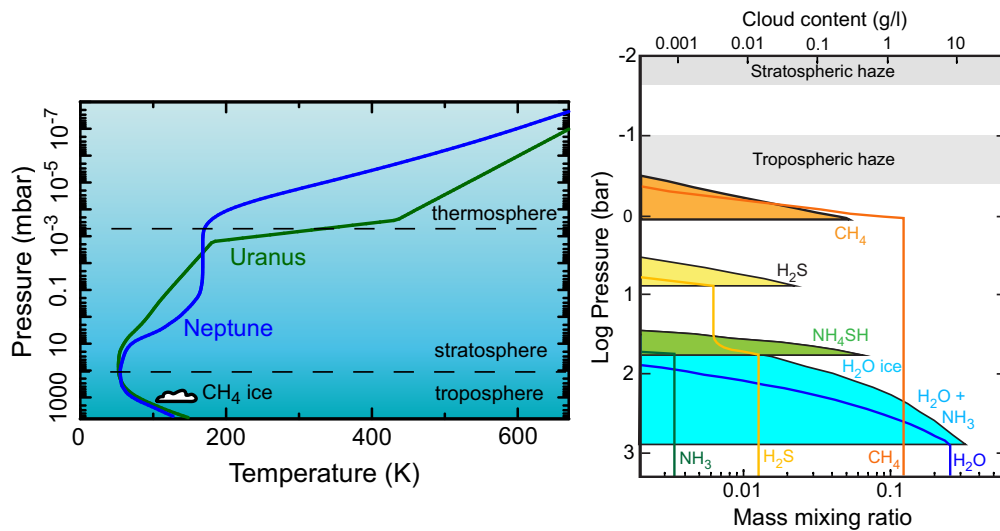


**Figure 1.** (Left) Global-average temperature-pressure profile of the atmospheres of Uranus and Neptune, with major regions of the atmosphere labeled (modified from Moses et al. [21]). (Right) Thermochemical equilibrium prediction of the upper-tropospheric cloud structure on Uranus (modified from Hueso and Sánchez-Lavega [22]). The predicted mass mixing ratios of condensable gases are shown as colored solid lines, and the maximum cloud density as solid black lines with color-shaded regions.

Observations at various wavelengths can probe down to the few-bar level in the upper troposphere, but gas and cloud opacity and Rayleigh scattering limit the penetration any deeper [22]. The expected upper-tropospheric cloud structure from thermochemical-equilibrium arguments is shown in Fig. 1, as is described in Hueso et al. [22]. This figure illustrates the cloud structure for Uranus, but the results for Neptune are similar. In this thermochemical-equilibrium scenario, a liquid water and ammonia solution cloud forms at the several-hundred bar level, transitioning to a water-ice cloud near its top. Gas-phase  $H_2O$  is strongly depleted in this region as the water condenses. Above the water cloud, ammonia ( $NH_3$ ) and hydrogen sulfide ( $H_2S$ ) can combine to form an ammonium hydrosulfide ( $NH_4SH$ ) cloud, substantially depleting whichever gas phase species is less abundant. Observations of both Uranus and Neptune suggest that  $H_2S$  is

more abundant than  $\text{NH}_3$  [23–28]. The remaining  $\text{H}_2\text{S}$  then forms an  $\text{H}_2\text{S}$  ice cloud at the several-bar level, and methane ( $\text{CH}_4$ ) then condenses as an ice cloud near the  $\sim 1$ -bar level. Various optically thin hazes from disequilibrium species and photochemical products reside above the  $\text{CH}_4$  cloud. Below the water cloud, other equilibrium cloud layers are predicted to form [29,30], depleting the atmosphere in refractory elements above their condensation regions. In fact, of all the equilibrium species predicted to be present in the atmospheres of Uranus and Neptune, only  $\text{H}_2$ , He,  $\text{CH}_4$ , and  $\text{H}_2\text{S}$  are directly detected spectroscopically, while everything else that has been observed is believed to be produced from disequilibrium chemical processes.

**Table 1.** Tropospheric composition by volume (above the water-solution cloud) from selected recent references

species	Uranus	Neptune	notes/references
He	15.2%	14.9%	[31,32]
$\text{CH}_4$	1.4–4%	2–5%	latitude dependent; [33–36]
$\text{NH}_3$	30–90 ppm	40–200 ppm	inferred from microwave photometry; [25,37,38]
$\text{H}_2\text{O}$	< 5% *	27% *	*indirect determination of deep abundance; [39,40]
$\text{PH}_3$	< 2 ppm	< 1.1 ppb at 0.7 bar	[41,42]
$\text{H}_2\text{S}$	0.4–0.8 ppm > 10–25 ppm	1–3 ppm 700 ppm	at $\text{H}_2\text{S}$ cloud top; [26,27] below $\text{H}_2\text{S}$ cloud (latitude dependent); [26,28]

**Table 2.** Stratospheric composition by volume from selected recent references

species	Uranus	Neptune	notes/references
$\text{CH}_4$	16 ppm at 50 mbar	0.115% at 5 mbar	[43,44]
$\text{C}_2\text{H}_2$	0.25 ppm at 0.2 mbar	0.033 ppm at 0.5 mbar	[45,46]
$\text{C}_2\text{H}_4$	< $2 \times 10^{-14}$ at 10 mbar	0.8 ppb at 0.2 mbar	[45,47]
$\text{C}_2\text{H}_6$	0.13 ppm at 0.2 mbar	0.85 ppm at 0.3 mbar	[45,48]
$\text{C}_3\text{H}_4$	0.36 ppb at 0.4 mbar	0.12 ppb at 0.1 mbar	[45,49]
$\text{C}_4\text{H}_2$	0.13 ppb at 0.4 mbar	0.003 ppb at 0.1 mbar	[45,49]
$\text{CO}_2$	0.08 ppb at 0.14 mbar	0.78 ppm at 0.1 mbar	external source; [45,49]
CO	6 ppb at 0.5 mbar	1.1 ppm at 0.1 mbar	external source; [50,51]
$\text{H}_2\text{O}$	3.8 ppb at 0.03 mbar	2.5 ppm at 0.16 mbar	external source; [52]
D/H	$4.4 \times 10^{-5}$	$4.1 \times 10^{-5}$	from HD; [53]

The atmospheric constituents observed during the *Voyager 2* era and earlier are discussed in several reviews [15–19]. Since that time,  $\text{H}_2\text{S}$  has been definitively detected in the troposphere of Uranus and tentatively on Neptune [26,27], several new disequilibrium products and exogenic species have been detected throughout the atmosphere [45,47,49,52,54–61], and refinements to previous abundance measurements have been reported [28,32–34,41–44,46,48,50,51,53,62–90]. Some spatially resolved information on species abundances has also become available in recent years [26–28,33–36,46,84,86,90–96]. Table 1 and Table 2 summarize the observed abundance of tropospheric and stratospheric constituents on the Ice Giants. Values in these tables have been chosen from a single reference observation per planet; for additional observations and more in-depth discussions of uncertainties, see the full suite of references listed above.

### 3. Tropospheric chemistry

Thermochemical equilibrium dominates the chemistry in the deep troposphere on Uranus and Neptune, and transport-induced quenching and photochemistry affect the upper troposphere.

### (a) Thermochemical equilibrium and quenching

Deep in the tropospheres of Uranus and Neptune at pressures greater than several kilobar, temperatures are high enough and reaction rates are fast enough that thermochemical equilibrium can be maintained. The deep tropospheric composition can then be predicted as a function of pressure, temperature, and elemental abundances by assuming thermochemical equilibrium [29,30]. However, gas that is transported upward from the deep troposphere will cool, and the colder temperatures will inhibit some chemical reactions (e.g., those with high-energy barriers), such that thermochemical equilibrium will eventually cease to be maintained kinetically. When the rate of vertical transport exceeds the rate at which chemical reactions convert between different molecular forms of an element, then the composition can be “frozen in” at that stage [97], producing vertically uniform mixing ratios of the involved species above the quench point, in the absence of any other chemical processes such as photochemistry or condensation. As a consequence of this disequilibrium transport-induced quenching process, species such as CO, N<sub>2</sub>, PH<sub>3</sub>, GeH<sub>4</sub>, C<sub>2</sub>H<sub>6</sub>, HCN, HCl, HF, CO<sub>2</sub>, CH<sub>3</sub>OH, CH<sub>3</sub>SH, CH<sub>3</sub>NH<sub>2</sub>, and H<sub>2</sub>Se are expected to survive into the upper troposphere of Uranus and Neptune at abundances much greater than equilibrium predictions [30]. Because the quenched abundances depend on the bulk elemental abundances in the deep atmosphere, as well as the strength of atmospheric mixing, these disequilibrium species are potentially important indicators of conditions in the deep tropospheres of the Ice Giants, where both *in situ* probes and remote-sensing observations cannot penetrate. Of the aforementioned disequilibrium species, only carbon monoxide (CO) has been definitively detected in the *troposphere*, and only on Neptune [42,51,54,55,65,67,85]. However, even upper limits for these species can provide important information about the deep atmosphere [17].

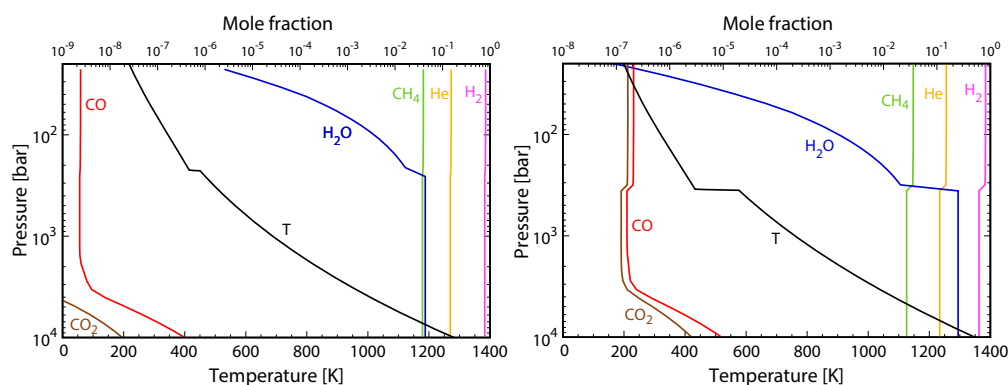


**Figure 2.** Mole fraction profiles of some key species in the deep troposphere of Uranus (Left) and Neptune (Right), as predicted from a thermochemical kinetics and diffusion model [39,40]. The deep carbon and oxygen abundances are varied until the model reproduces the observed upper tropospheric CH<sub>4</sub> mixing ratio at the equator [33,34] and the observed upper-tropospheric CO mixing ratio (Neptune) or CO upper limit (Uranus) [51,85]. Figure modified from Venot et al. [39].

Carbon monoxide has also been detected in the stratospheres of Uranus and Neptune with a mixing ratio greater than is found in the troposphere [50,65,67,85], indicating that CO has an external source on these planets. However, tropospheric CO can also result from an internal, deep quenched source. The observed upper-tropospheric CO volume mixing ratio on Neptune is surprisingly large, but somewhat uncertain — various reports put it in the 0.08–1.5 ppm range [41,42,48,51,54,55,62–69]. The uncertainty arises from observational difficulties and model dependencies in the fitting of the pressure-broadened wings of the CO absorption features. In contrast, the most stringent upper limit for tropospheric CO on Uranus is as low as  $2.1 \times 10^{-9}$  [85] — a low value that presumably results from Uranus’ expected less efficient

tropospheric mixing (as supported by its low internal heat flux [103]) and potentially smaller intrinsic deep oxygen abundance [39,40]. Observational constraints on the tropospheric CO abundances on Uranus and Neptune have been used to constrain the deep O/H abundance on these planets, assuming that the CO derives from quenching from the deep interior [17, 39,40,50,51,98]. Early estimates via time-scale arguments [17,51,55,98] have given way to more complete thermochemical kinetics and transport models [39,40,50], based on those developed for Jupiter and extrasolar planets [99–102]. The full suite of these estimates suggests a deep oxygen enrichment relative to hydrogen on Neptune of 250–650 times solar, while the upper limit for Uranus is < 45–260 times solar.

Figure 2 shows the predicted vertical profiles of a few species in the deep troposphere of Uranus and Neptune from the nominal thermochemical kinetics and diffusion model of Venot et al. [39], updated from Cavalié et al. [40]. Both planets are assumed to have a deep-tropospheric eddy diffusion coefficient  $K_{zz} = 10^8 \text{ cm}^2 \text{ s}^{-1}$  in this model, as estimated from mixing-length theory (for which  $K_{zz}$  varies with the internal heat flux to the one-third power, so the factor of  $\sim 10$  difference in the internal heat flux of the two planets translates to only a factor of  $\sim 2$  difference in  $K_{zz}$ , although it is possible that convection is inhibited on Uranus [103], making  $K_{zz}$  even smaller). Venot et al. find that a deep O/H abundance of 250 times solar for Neptune and < 45 times solar for Uranus are needed to reproduce the upper-tropospheric observational constraints for CO [51,85]. As discussed below, this solution is somewhat model dependent. Other interesting features of the deep tropospheres of the Ice Giants are apparent from Fig. 2. The large discontinuity that appears in the temperature profile and species abundances in the middle troposphere is a result of water condensation. Water is a major component of the Ice Giants, and when  $\text{H}_2\text{O}$  is removed from the gas phase due to condensation, the mixing ratios of all the remaining gas-phase species — including  $\text{H}_2$  — increase notably. The mean molecular mass of the atmosphere also drops significantly when  $\text{H}_2\text{O}$  condenses, which can produce a stable layer that inhibits convection [40,104]. These types of models also predict the quench behavior of  $\text{CO}_2$ ,  $\text{CH}_3\text{OH}$ ,  $\text{N}_2$ ,  $\text{HCN}$ , and other constituents [39,40,50,100,102,105], which could in theory supply additional constraints on the deep elemental abundances and/or vertical transport rates if these species are ever detected in Ice-Giant tropospheres [17].

Thermochemical kinetics and transport models therefore have the potential for being a powerful tool for indirectly determining the bulk elemental atmospheric abundances on the Ice Giants (see also the review of Cavalié et al. [106]). Many of the assumptions and inputs to these models are uncertain, however, adding significant uncertainties to the final result. For example, the model results are sensitive to the thermal structure of the deep atmosphere, which is not well constrained and must be extrapolated many orders of magnitude from sparse measurements from the upper troposphere, and which is affected by complicated and often poorly characterized physical and chemical effects (e.g., non-ideal gas effects, critical-point behavior, wet-versus-dry adiabats, double-diffusive convection, the atmospheric evolution history, 3D dynamical effects) [40,98,104]. Vertical transport is typically parameterized through an eddy diffusion coefficient profile in these models, which can depend on the internal heat flux, temperature profile, and composition profile, and is predicted to be latitude dependent [99,107,108]. The model results are also very sensitive to individual chemical reaction rates involved in the conversion between different forms of an element, the uncertainties of which can lead to potential order-of-magnitude uncertainties in the predicted abundance of quenched species [102,109,110]. When Venot et al. [39] updated the reaction mechanism used in Cavalié et al. [40], for instance, their revisions led to a reduction in their previously predicted values of the deep oxygen abundance by a factor of 2 for Neptune and a factor of 3.5 in the upper limit for Uranus. Judging from comparisons with other combustion-based and atmospheric-based kinetics models [109,110], the uncertainties in the deep O/H abundance that result from kinetics uncertainties could be even larger than this factor of a few. However, if the above model uncertainties could be reduced, this indirect means of determining deep elemental abundances on the Ice Giants holds much promise, particularly

if future observations and missions are able to measure the tropospheric abundance of multiple disequilibrium quenched species [106,111].

### (b) Tropospheric photochemistry

Longer-wavelength ultraviolet photons from the Sun can reach the upper troposphere to initiate local photochemistry, although Rayleigh scattering and aerosol extinction ultimately limit how far the photons can penetrate. Tropospheric photochemistry on Uranus and Neptune has not received much attention, in part because of a lack of observational motivators. Although phosphine ( $\text{PH}_3$ ) — believed to be a disequilibrium quenched species that should be the dominant form of phosphorous in the upper troposphere [29] — can condense in the cold upper tropospheres of Uranus and Neptune,  $\text{PH}_3$  may be photolyzed and destroyed before condensation can occur. The resulting photochemistry would lead primarily to the formation of  $\text{P}_2\text{H}_4$  hazes, as has been suggested for Saturn [112]. Indeed,  $\text{PH}_3$  photolysis is efficient in the recent Neptune tropospheric photochemical model presented by Teanby et al. [42] and can easily explain their low derived 1.1 ppb upper limit for  $\text{PH}_3$  near 0.4–0.8 bar. Why, then, does photolysis not remove  $\text{PH}_3$  from view on Jupiter and Saturn? The difference in upper tropospheric  $\text{PH}_3$  abundance on these planets is the result of enhanced shielding of the  $\text{PH}_3$  from photolysis on Jupiter and Saturn due to the presence of  $\text{NH}_3$  gas and cloud particles in the upper troposphere, whereas  $\text{NH}_3$  has already been removed at deeper pressures on Neptune (see Fig. 1). The rate of vertical mixing in the upper tropospheres of these planets may also play a role. The derived  $\text{PH}_3$  profile from the Teanby et al. model suggests that any atmospheric probe would need to go to at least 10 bar to have a chance of sampling the deep phosphorus abundance, due to the vertical gradient imposed by strong photochemical loss, slow mixing, and potential condensation in the radiative portion of the upper troposphere. The expected low  $\text{NH}_3$  abundance in the 1–3 bar pressure region where  $\text{PH}_3$  is being photolyzed (see Fig. 1) limits the importance of the coupled  $\text{NH}_3$ – $\text{PH}_3$  photochemistry that is suggested to occur on Jupiter and Saturn [113,114]. Similarly, the expected low abundance of hydrocarbon radicals and unsaturated hydrocarbons in the region where  $\text{PH}_3$  is being photolyzed limits the coupling of  $\text{PH}_3$  and hydrocarbon photochemistry. Under favorable conditions of strong convective uplift,  $\text{H}_2\text{S}$  may be carried to high-enough altitudes to interact with photons of less than  $\sim 260$  nm, which can photolyze the  $\text{H}_2\text{S}$ . Under these rare but interesting conditions, sulfur photochemistry might occur. The details of  $\text{H}_2\text{S}$  photochemistry under reducing conditions are poorly understood, due to a lack of relevant chemical kinetics data, but condensed elemental sulfur is a potential end product of this chemistry.

### (c) Tropospheric latitude variations

In recent years, observations have demonstrated that tropospheric condensible species such as  $\text{CH}_4$  and  $\text{H}_2\text{S}$  have abundances that vary with latitude on both Uranus and Neptune [26–28,33–36,84,90,91,93,95,96] (see Fig. 3). These species have strong, broad-scale, equator-to-pole mixing-ratio gradients, with higher abundances at low latitudes than high latitudes, and some evidence for meridional variability on smaller scales. In contrast, spatially resolved observations of Jupiter and Saturn show variations in tropospheric  $\text{NH}_3$  that occur on more local scales due to the belt-zone structure [115–121]. Latitude variations in tropospheric condensible species could be common on all the giant planets, with the *Juno* observations in particular demonstrating that abundances can be variable to much deeper pressures than previously realized [117,118,122]. The complete vertical profiles of  $\text{CH}_4$  and  $\text{H}_2\text{S}$  on Uranus and Neptune as a function of latitude have not yet been worked out, nor have  $\text{NH}_3$  and  $\text{H}_2\text{O}$  been definitively detected. An important goal for future observations and missions is the determination of how the temperatures and the gas-phase abundances of these condensible species vary in a three-dimensional sense. The distributions of condensible species are intimately linked to atmospheric dynamics. The observed variation is useful for determining broad-scale atmospheric circulation on the Ice Giants [94,123,

124], as well as for furthering our understanding of how convection originates and operates in hydrogen-dominated atmospheres for which the condensate is heavier than the background gas [125]. Moist air in H<sub>2</sub>-dominated atmospheres will tend to sink rather than rise, but latent-heat release from condensation [126,127] and energy release from ortho-para H<sub>2</sub> conversion [128] can fuel storms. How moist convection is initiated in the methane cloud layer on the Ice Giants is not immediately obvious [22,127,129], nor is it clear how important localized storms are compared to broader circulation in controlling condensable species abundances, atmospheric structure, and energy transport on hydrogen-dominated planets [118,121,123–125,130–132].

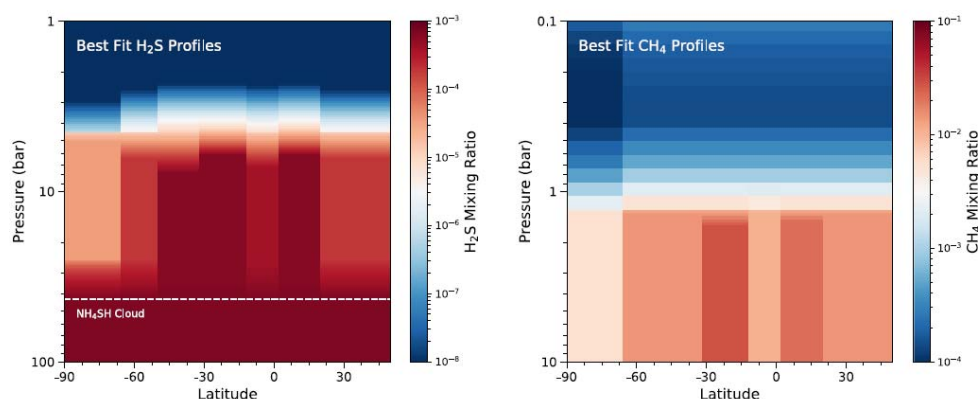


**Figure 3.** Mixing ratios of H<sub>2</sub>S (Left) and CH<sub>4</sub> (Right) as a function of latitude on Neptune from models that provide the best fits to the ALMA data of Tollefson et al. [28]. Figure from [28].

Latitude and other spatial variations complicate analyses of remote-sensing data and plans for future deep-probe missions. The degeneracy between temperatures and species abundances in atmospheric retrievals will be even more difficult to break when both are non-uniform across the planet. Given that species abundances vary spatially, where do we want to send potential probe(s)? How deep do the probes need to go to sample the well-mixed deep abundance of different species?

Tropospheric species that neither condense nor participate in active chemistry (e.g., noble gases and chemically long-lived species) are expected to have mixing-ratio profiles that are constant with altitude and latitude. This theoretical expectation is not backed up by any current observations, but with no known production or loss processes, there is no apparent way to alter the volume mixing ratio in a background gas that remains stable. Exceptions to this prediction are quenched disequilibrium species such as CO and N<sub>2</sub>, whose mixing ratios could potentially vary with latitude as a result of meridional variations in the convective transport rates in the deep troposphere that affect the quench location [110]. Tropospheric constituents that might not vary with latitude on Uranus and Neptune, such as noble gases and their isotopes, are prime targets for measurements on future probe missions [133]. The relative abundance of these gases can help identify the origin of the heavy elements in the Ice Giant atmospheres from various possible reservoirs in the protosolar nebula [7,9,133]. Molecular nitrogen (N<sub>2</sub>) and CO are important quenched species from the deep atmosphere that would help constrain the deep N/H and O/H abundances. Given that CO has the same molecular weight as N<sub>2</sub>, and the two would be indistinguishable from each other in a low-resolution mass spectrometer, a probe that has instrumentation that could differentiate between N<sub>2</sub> and CO would be ideal.

## 4. Stratospheric chemistry

Despite the weak solar ultraviolet flux in the outer solar system, photochemistry on Uranus and Neptune is quite active and vigorous. Methane photolysis initiates the stratospheric photochemistry on these planets, producing a slew of hydrocarbon photochemical products [16,18], many of which are observed (see Table 2). Seasonal changes in solar forcing are expected to lead to temporal and spatial differences in stratospheric chemistry. Surprising discrepancies in the abundance of photochemical products between the two planets point to significant differences in the strength of atmospheric mixing [21,134–136]. External material coming into the atmosphere from interplanetary dust particles, comets, and the local satellite/ring system contributes to stratospheric chemistry [52].

### (a) Methane photochemistry

Although methane condenses in the upper troposphere of both planets, sufficient  $\text{CH}_4$  is transported up into the stratosphere — by moist convection or other processes that are not well understood — where the methane can interact with solar photons of wavelengths less than  $\sim 145$  nm, triggering photolysis. Photochemical models for the stratospheres of Uranus and Neptune have been presented by several groups [21,45,47,50,58,70,72,74,135,137–150]. These models indicate that a variety of hydrocarbons are produced from stratospheric methane photochemistry, including methyl radicals ( $\text{CH}_3$ ), acetylene ( $\text{C}_2\text{H}_2$ ), ethylene ( $\text{C}_2\text{H}_4$ ), ethane ( $\text{C}_2\text{H}_6$ ), methylacetylene ( $\text{CH}_3\text{C}_2\text{H}$ ), and diacetylene ( $\text{C}_4\text{H}_2$ ), which have been observed on one or both of these planets (see Table 2). These products and others can be photolyzed themselves, leading to a complex and intricate hydrocarbon kinetics that has many similarities to that on Jupiter and Saturn (see the reviews of [113,114]). The photochemical products will flow down from the methane photolysis region in the upper stratosphere to the lower stratosphere, where many of the products can condense to form hazes, as are observed in the  $\sim 1$ –100 mbar region [144,151,152]. Ethane, acetylene, and diacetylene are the dominant photochemical components of this haze, but other hydrocarbons and externally supplied species such as  $\text{H}_2\text{O}$ ,  $\text{CO}_2$ , and  $\text{HCN}$  — the latter which could also derive from cosmic-ray dissociation of internal  $\text{N}_2$  or from N from Triton [55,72] — also contribute to the stratospheric aerosol.

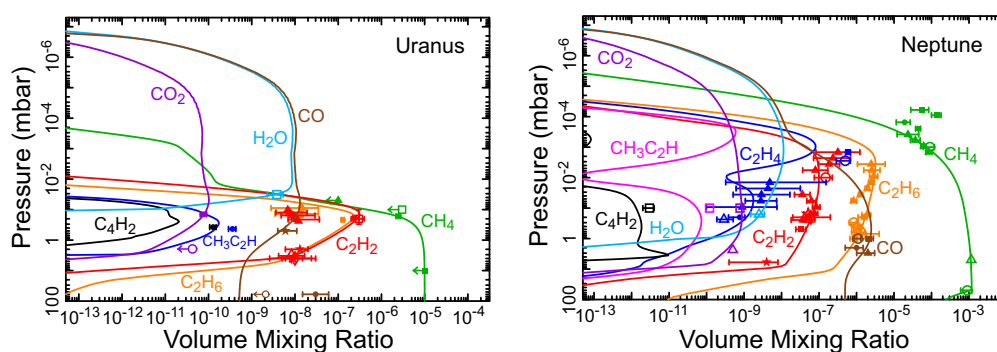


**Figure 4.** Vertical mixing-ratio profiles for several stratospheric constituents on Uranus (Left) and Neptune (Right) as predicted from 1-D global-average photochemical models (colored lines), compared to various observations (data points with associated error bars). The models for both planets include an external source of oxygen from the ablation of interplanetary dust [148], while the Neptune model includes a source of CO from a large cometary impact 200 years ago. The sharp drops in species mixing ratios in the lower stratosphere are caused by condensation. Figure modified from Moses and Poppe [148].

Key differences between the photochemical product abundances on Uranus and Neptune arise predominantly from differences in the strength of stratospheric mixing between the two planets (see Fig. 4), which results from the presence and strength of atmospheric waves (including breaking gravity waves), circulation and winds, and turbulence of all scales. Mixing is weak on Uranus but strong on Neptune. The stronger mixing on Neptune allows  $\text{CH}_4$  to be carried to much lower pressures (higher altitudes) than on Uranus (see Fig. 4), before the homopause level is attained and molecular diffusion dominates, causing species such as methane and its photochemical products that are heavier than the background  $\text{H}_2$  to drop off sharply with altitude. The higher homopause altitude on Neptune allows the photochemical products to build up over a much larger vertical column above their condensation regions in the lower stratosphere than on Uranus. The column abundances of photochemically produced hydrocarbons therefore tend to be larger on Neptune, and are easier to observe than on Uranus — Neptune observations are also aided by a larger temperature gradient and warmer stratosphere. The pressure at which  $\text{CH}_4$  is photolyzed also affects the subsequent photochemistry [45,146], leading to differences in the relative abundances of the hydrocarbon products on Uranus versus Neptune.

Detailed descriptions of neutral hydrocarbon photochemistry on Uranus and Neptune are provided in [21,45,146,150]. Dobrijevic et al. [147] discuss how uncertainties in reaction rate coefficients propagate to uncertainties in hydrocarbon abundances in photochemical models. Model uncertainties are as large or larger than observational uncertainties for many species.

### (b) Dependence on latitude and season

The abundance of hydrocarbon photochemical products on Uranus and Neptune depends on latitude and season. Uranus' extreme axial tilt of  $97.8^\circ$  and Neptune's more moderate axial tilt of  $28.3^\circ$  cause seasonal variations in the solar actinic flux that drives photochemistry on the Ice Giants. This obliquity, combined with the long orbital periods of the planets, ensures strong and long-lasting differences in the production and loss rates of hydrocarbons over time. Portions of Uranus and Neptune experience many Earth years of darkness during winter, with only a small amount of solar Lyman alpha radiation scattered from hydrogen in the local interplanetary medium providing any source of photolyzing radiation. Averaged over of a full planetary year, the poles of Uranus receive a greater flux of ultraviolet radiation than the equator, while the opposite is true for Neptune. This seasonally variable solar forcing results in meridional gradients in photochemical product abundances that change with time and altitude. Two-dimensional or three-dimensional time-variable models are needed to track this variation (e.g., [153] for Jupiter). Moses et al. [21] have presented such two-dimensional time-variable photochemical models for Uranus and Neptune, under the assumption of rapid zonal homogenization and no meridional transport.

Figure 5 illustrates how the column abundance of two photochemically produced hydrocarbons,  $\text{C}_2\text{H}_2$  and  $\text{C}_2\text{H}_6$ , are expected to vary with latitude and season on Neptune from the Moses et al. [21] model. At very high altitudes (not shown), chemical and transport time scales are short, and the atmosphere responds quickly to changes in the solar actinic flux. The greater flux during the summer season leads to greater hydrocarbon production rates, and a generally higher abundance of photochemical products. Conversely, hydrocarbon abundances drop off significantly during the long, dark winter at high latitudes. Seasonal variations in abundance are greatest at low pressures, but are reduced at depth as a result of diffusion and chemical time scales that increase with increasing pressure. The greater time constants at higher pressures cause phase lags in the response to seasonal solar forcing, as can be seen in Fig. 5. Similarly, the meridional distribution of photochemical products becomes more symmetric about the equator at pressures greater than a few millibars — time constants that are longer than a Neptune season cause the annual average solar actinic flux to be more important in controlling abundances than the time-variable seasonal forcing at these pressures. Seasonal differences in mixing ratios typically disappear at the few mbar level on Neptune or by  $\sim 1$  mbar on Uranus, although these values depend on latitude and the species in question [21].

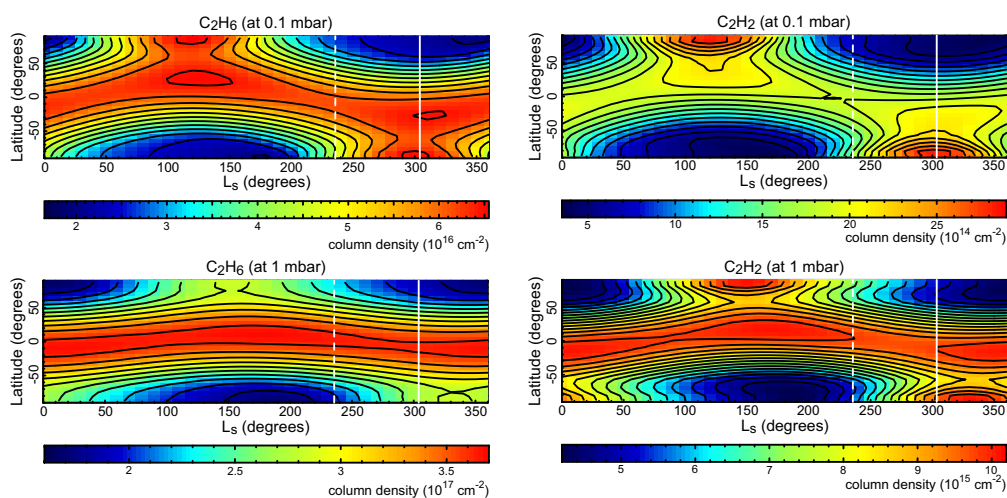


**Figure 5.** Photochemical model predictions [21] for the column abundance of  $C_2H_6$  (Left) and  $C_2H_2$  (Right) above 0.1 mbar (Top) and 1 mbar (Bottom) on Neptune as a function of planetocentric latitude and season, where the season is represented by solar longitude  $L_s$  ( $L_s = 0^\circ$  is northern vernal equinox,  $L_s = 90^\circ$  is northern summer solstice, etc.). The white dashed line shows the season at the time of *Voyager 2* encounter, and the white solid line shows the season at the current expected launch date (March 30, 2021) for the *James Webb Space Telescope (JWST)*. Figure modified from Moses et al. [21].

Surprisingly, seasonal variations in photochemical product abundances are expected to be weaker on Uranus than on Neptune [21], despite the greater obliquity of Uranus. These weaker seasonal variations result from the weaker stratospheric vertical mixing on Uranus that confines methane to relatively deep pressure levels in the stratosphere. Both the vertical transport time scales and chemical time scales are long in the region where  $CH_4$  is photolyzed on Uranus, so the hydrocarbon photochemical products do not respond quickly to the variable solar forcing. However, in the 0.1–1 mbar region that is probed by mid-infrared observations, some seasonal variations are expected, leading to north vs. south hemispheric dichotomies in the photochemical product abundances during most seasons [21]. Species such as  $C_2H_2$ ,  $C_3H_4$ , and  $C_4H_2$  are predicted to exhibit a maximum at the poles in the summer-to-fall hemisphere due to both the annual-average solar insolation being greater at high latitudes than at low latitudes and to the phase lags in the response to the seasonally variable insolation. In contrast,  $C_2H_6$  is predicted to have a maximum at low latitudes because loss by photolysis effectively competes with production in the high-latitude summer.

For Saturn, comparisons between the predicted and observed meridional distributions of temperatures and hydrocarbon abundances helped identify certain characteristics of stratospheric transport, such as regions of local upwelling and downwelling that can help define stratospheric circulation patterns [154–171]. The same could be true for Uranus and Neptune. Observations that define the meridional variations in photochemical product abundances have recently become available for Uranus [96] and Neptune [46,86]. The meridional distributions of  $C_2H_2$  and  $C_2H_6$  predicted by the Neptune photochemical model of Moses et al. [21] appear to compare well to the limited available observations [46,86], suggesting that stratospheric transport has a more minor effect on species abundances at Neptune than it does at Saturn. Further observations that map out species abundances as a function of altitude, latitude, and time are needed to confirm this claim.

In contrast, Uranus exhibits strong changes in brightness temperature with latitude at 13  $\mu\text{m}$  [96] that are not predicted by the seasonal model. Under the assumption that the brightness-temperature variations result solely from changes in the mixing ratio of  $C_2H_2$  rather than variations in temperature (i.e., recall the degeneracy between temperatures and abundances in

analyses of emission data), the  $C_2H_2$  mixing ratio at  $\sim 0.2$  mbar has a minimum at the equator in observations from 2009 ( $L_s \approx 7^\circ$ ), with a maximum at mid-latitudes in both the northern and southern hemispheres [96]. That pattern does not change much in observations acquired in 2018 ( $L_s \approx 46^\circ$ ), where the equatorial minimum and northern mid-latitude local maximum are still seen (southern mid-latitudes are no longer in view) [96]. The inferred  $C_2H_2$  abundances at mid- and high-latitudes are roughly consistent with model predictions, but the observed variations with latitude are far greater than predicted, and the equatorial minimum and local maximum at northern mid-latitudes are unexpected.

This mid-latitude peak in emission could potentially be produced by a local maximum in stratospheric temperatures, perhaps caused by a downwelling with consequent adiabatic heating. However, retrievals of upper-tropospheric temperatures suggest a tropospheric upwelling at these same mid-latitudes, so the stratospheric circulation would have to be in the opposite sense to that in the troposphere. Roman et al. [96] put forth an alternative explanation, suggesting that the relative enhancement at northern mid-latitudes could be caused by stronger stratospheric mixing at these latitudes (due to the tropospheric upwelling) that carries more methane to higher altitudes, allowing more  $C_2H_2$  to be photochemically produced at these latitudes compared to the equatorial region, especially as the solar actinic flux is beginning to increase as summer approaches. Preliminary modeling suggests that such enhancements would require considerable changes to the column abundances and vertical profiles of all hydrocarbons at these latitudes. Regardless of whether either explanation is responsible, the discrepancy between current models and observations of Uranus is intriguing and might provide useful insight to coupled tropospheric-stratospheric dynamics and coupled stratospheric dynamics and chemistry. To make further advances in this topic, an additional way to break the strong degeneracies between temperatures and abundances in mid-infrared emission observations would be valuable (e.g., spatially resolved measurements of the S(1) quadrupole line of  $H_2$  — as will be possible with *JWST* [172] — to help constrain stratospheric temperatures, *in situ* temperature measurements from probe(s), better derivations of stratospheric  $CH_4$  vertical and meridional distributions at visible and near-infrared wavelengths that are not so degenerate with temperature), as would additional observations that target the stratospheric distributions of hydrocarbons.

### (c) Effects of external material

Oxygen-bearing species such as  $H_2O$ ,  $CO_2$ , and  $CO$  are present in the stratospheres of Uranus and Neptune [42,45,48–52,65,67,85]. Any  $CO_2$  and  $H_2O$  being carried up from the deep troposphere on Uranus and Neptune would be expected to condense long before reaching the stratosphere, and although  $CO$  does not condense and can have a deep tropospheric source, the fact that the mixing ratio of  $CO$  is greater in the stratosphere than the troposphere on both planets indicates a source from outside the planet. Delivery of oxygen from the ablation of interplanetary dust particles is the right order of magnitude to explain the observed amount of  $H_2O$ ,  $CO_2$ , and  $CO$  in the stratosphere of Uranus [148,173], but cometary impacts or local satellite/ring material could also contribute [50,148,149]. For Neptune, the expected dust influx rates are far too small to explain the large observed amount of  $CO$  in Neptune's stratosphere, pointing to a very large cometary impact within the last  $\sim 1000$  years [51,61,65,67,148,150,173]. The large  $CO$  amount, plus its greater mixing ratio in the stratosphere than the troposphere, the large inferred stratospheric  $CO/H_2O$  ratio, and the observed presence of stratospheric hydrogen cyanide ( $HCN$ ) [54,55,62,66,72] originally led Lellouch et al. [65] to suggest that the  $CO$  was delivered to Neptune through a large cometary impact a few hundred years ago. Recent carbon monosulfide ( $CS$ ) observations [61] strengthen this cometary-impact possibility.

Depending on the source of the external material, the oxygen species will be delivered to Uranus and Neptune at different pressure levels. For gas coming in from a local satellite or ring source, the oxygen can flow in from the top of the atmosphere, affecting chemistry throughout the atmosphere. For an interplanetary dust source [173], ablation of icy grains releases oxygen-bearing species to the  $\sim 10^{-1}$  to  $10^{-7}$  mbar region of Uranus and Neptune [148,174], which

affects chemistry both above and below the methane homopause. Observations and models of the impacts of Comet Shoemaker-Levy 9 with Jupiter taught us a lot about how comet-derived material ends up in planetary stratospheres [175–177]. During a large cometary impact, vaporized cometary material plus some ambient gas from the terminal explosion deeper in the atmosphere will rush back up the entry column to form a plume of material that rises above the atmosphere before falling back upon the stratosphere [178,179]. During this plume splashback phase, the material that re-enters the atmosphere is reshocked (resetting the molecular composition) and deposited within the middle stratosphere [175,176,179,180]. The plume re-entry shock from the Shoemaker-Levy 9 impacts was characterized by relatively low shock pressures and high temperatures, with the maximum shock temperatures depending on the plume re-entry vertical velocity (and thus distance from the impact site) [175]. The fact that CO was favored over H<sub>2</sub>O at the impact sites suggested that typical peak re-entry shock temperatures were above  $\sim 1400$  K during the Shoemaker-Levy 9 impacts [175,176]. In general, CO was found to be a factor of  $\sim 10$ – $100$  more abundant than H<sub>2</sub>O in the Jovian stratosphere after the impacts [176,180,181], and the CO, HCN, and CS that were formed during the plume splashback phase have persisted for years in the Jovian stratosphere [182–186], as was predicted from photochemical models [177,187,188]. Observations suggest that these species were introduced at pressures less than  $\sim 0.1$  mbar after the impacts, and have been diffusing slowly downward since that time [180,182,189]. External species delivered to atmospheres of Uranus and Neptune from large cometary impacts are expected to have similar behavior, although the amount of material introduced and its initial vertical distribution will depend on the size of comet, as well as its entry velocity.

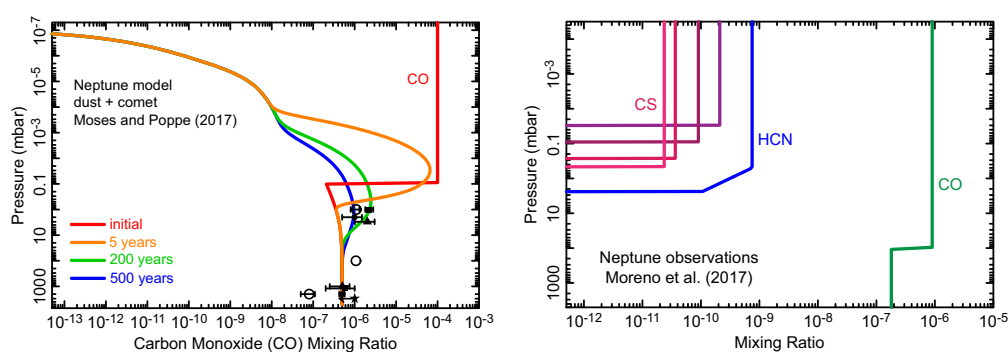


**Figure 6.** (Left) Photochemical model predictions for the time evolution of CO introduced from a large cometary impact on Neptune, along with a smaller steady source from the ablation of icy interplanetary dust grains (Figure modified from Moses and Poppe [148]). (Right) Mixing ratio profiles derived for CS, HCN, and CO from analyses of the millimeter and sub-millimeter observations of Moreno et al. [61] and Luszcz-Cook and de Pater [51]. Note that although the column abundance of CS is well constrained from the observations, the mixing-ratio profile is not, so multiple models are shown that all provide a good fit to the data [61] (Figure modified from Moreno et al. [61]).

Photochemical models can track the fate of the oxygen species introduced by these external sources [21,45,50,146,148–150,174] (see Fig. 6). Potential sources from dust ablation or the local satellite/ring systems can be modeled as continuous sources, while cometary impacts require time-variable models. In general, H<sub>2</sub>O, CO, and CO<sub>2</sub> are relatively stable chemically in the cold stratospheres of the Ice Giants. Chemical interactions with hydrocarbons do occur, but have only a minor effect on the abundances of the observable hydrocarbons. See Moses et al. [146,148,190], Orton et al. [45], Lara et al. [149], and Dobrijevic et al. [150] for a discussion of the photochemistry of oxygen species. If delivered in sufficient amounts, externally supplied H<sub>2</sub>O, CO<sub>2</sub>, and HCN will condense in the stratospheres of Uranus and Neptune, contributing to a high-altitude haze at pressures ranging from  $10^{-2}$  mbar (e.g., H<sub>2</sub>O on Uranus) to greater than 10 mbar (CO<sub>2</sub> on Neptune) (see Fig. 4).

The vertical distributions of CO, HCN, and CS on Neptune differ significantly from each other [61]. This interesting observation (see Fig. 6) could be the result of more than one large impact (with resulting vertical distributions that vary because of different ages or the size of the impactors), complicated and velocity-dependent plume splashback conditions, different rates of chemical loss for the different species, or a different external source altogether. The HCN, for example, could potentially derive from chemistry resulting from the dissociation of quenched disequilibrium  $N_2$  by galactic cosmic rays or by chemistry resulting from the inflow of nitrogen from Triton [19,54,55,72]. The chemistry of nitrogen species in Neptune's atmosphere has been explored previously [72], albeit not in the context of a cometary impact, but the fate of sulfur species delivered by a comet on Neptune has not yet been studied. The external material delivered to the Ice Giants could potentially affect ionospheric chemistry and structure, depending on the vertical distribution of the exogenic species [150,191].

Note from Fig. 6 that stratospheric CO from external sources is observed to extend down to at least 100 mbar pressure levels on Neptune [42,51], which suggests a very large impact occurred long enough ago ( $\gtrsim 1000$  years) for the comet-deposited material to have descended all the way to the tropopause [61]; alternatively, perhaps the external CO results from a more continuous influx of small comets, as has been suggested for Jupiter [192], or from local debris from the satellite/ring system. These scenarios lead to the uncomfortable possibility that the large amount of CO observed in the troposphere of Neptune could have a contribution from external sources, which would complicate the use of CO as an indirect indicator of the deep oxygen abundance.

## 5. Chemistry of the thermosphere and ionosphere

An ionosphere can form in the thermosphere and upper stratosphere of Uranus and Neptune from the interaction of the atmosphere with extreme ultraviolet radiation and X-rays. Galactic and solar cosmic rays can also ionize species down to tropospheric levels [194]. Ionospheric models of Uranus and Neptune have been developed by several groups [137,150,191,193–199]. Above the methane homopause at the top of the stratosphere, the ionosphere is dominated by  $H^+$  and  $H_3^+$ , which form the main ionospheric peak; some amount of  $H_3O^+$  and  $HCO^+$  is expected to be present, as well, depending on the external oxygen source and vertical profile. A secondary ionospheric peak forms in the lower thermosphere and upper stratosphere, populated by hydrocarbon ions (see Fig. 7). Ablated refractory debris from micrometeoroids could deliver metal vapors [174], whose long-lived atomic ions could potentially replace hydrocarbon ions in this secondary peak [191]. In fact, Lyons [191] suggests that sharp electron-density layering in the lower ionosphere of Neptune and the other giant planets, as seen from the *Voyager* radio occultation experiment, could be caused by  $Mg^+$  or other long-lived ions being compressed by horizontal winds with vertical shears (e.g., gravity waves) acting in the presence of the planet's magnetic field (see also [200,201]).

Of all the ionic species predicted to be present on the Ice Giants, only  $H_3^+$  has been detected, and only on Uranus [56,76,78,79,83,199,202–204]. Observations of  $H_3^+$  have provided a useful probe of thermospheric conditions on Uranus. For example, thermospheric temperatures derived from  $H_3^+$  observations have been observed to vary with time [83,204]. The long-term trends in thermospheric temperature variations are interesting and appear to be real. Moore et al. [193] caution that solar-zenith angle effects resulting from the changing seasonal geometry of the planet, combined with temperature gradients and  $H_3^+$  abundances that change with altitude, latitude, and local time, can influence derivations of thermospheric temperatures. Such global considerations should be taken into account when interpreting  $H_3^+$  observations. For the case of Neptune, ionospheric models typically predict  $H_3^+$  column densities greater than the observational upper limit [199]. The reasons for this discrepancy are not clear but may have to do with cooler thermospheric temperatures than were seen during the *Voyager* encounters, a larger than expected influx of external material interacting with the hydrogen ions and reducing their densities in favor of species like  $H_3O^+$  or  $HCO^+$ , or a methane homopause level that is higher in the atmosphere than was observed during the *Voyager* era (see Moore et al., this volume).

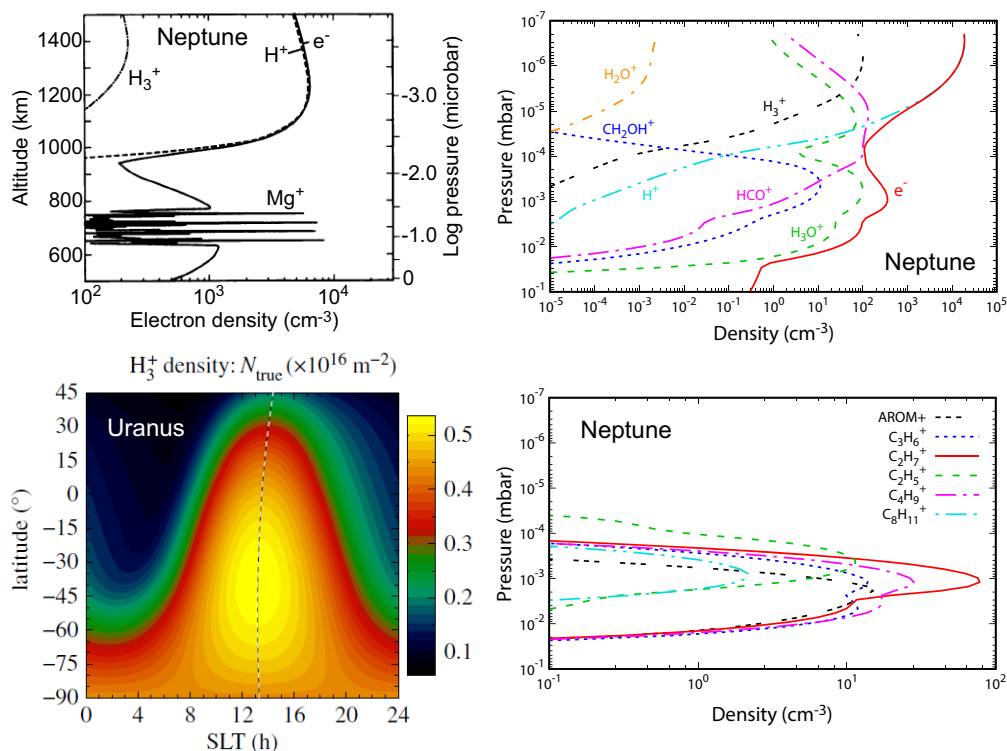


**Figure 7.** Ion chemistry on Uranus and Neptune: (Top Left) Photochemical model for Neptune's ionosphere, in which  $\text{Mg}^+$  ions form sharp layers in the lower ionosphere as a result of sinusoidal winds from a hypothetical atmospheric wave; figure modified from [191]. (Bottom Left) Global photochemical model results for Uranus, illustrating the  $\text{H}_3^+$  column density as a function of latitude and solar local time (SLT); figure from [193]. (Top Right) Photochemical model results for Neptune, illustrating the vertical profiles of major hydrogen and oxygen ions; figure from [150]. (Bottom Right). Photochemical model results for Neptune, showing the dominant hydrocarbon ions in the lower ionosphere; figure from [150].

Dobrijevic et al. [150] predict strong chemical coupling between ions and neutrals in the upper stratosphere of Neptune. They find that the production of neutral benzene and other aromatic hydrocarbons is enhanced several orders of magnitude by coupled ion-neutral chemistry, while  $\text{C}_2\text{H}_6$  is unaffected, and the abundance of  $\text{C}_2\text{H}_2$  is decreased by a factor of  $\sim 1.5$ . Neutral oxygen species such as  $\text{CO}_2$  are also affected by ion chemistry [150]. These predictions remain to be tested observationally — ultraviolet occultations (e.g., [205]) and mid-infrared limb spectra (e.g., [206]) from an orbiting spacecraft could provide useful tests of such models.

## 6. Conclusion and summary of outstanding science questions

Observations and models to date have revealed some crucial insights about atmospheric composition on Uranus and Neptune, but there is much we still do not know about atmospheric chemistry on our solar system's Ice Giants. Several photochemical products have been detected, along with a few equilibrium “parent” molecules such as  $\text{H}_2$ ,  $\text{CH}_4$ , and  $\text{H}_2\text{S}$ , but we have little information about the vertical and horizontal distributions of atmospheric constituents. Information about temporal variability is equally limited. Many elements are tied up in condensates at depths, preventing direct determinations of the bulk elemental composition. Degeneracies in observational analyses — such as between temperatures and constituent abundances in thermal emission observations (at wavelengths from the infrared to microwave)

and between constituent abundances and aerosol extinction in reflected sunlight observations (at ultraviolet, visible, and near-infrared wavelengths) — hamper the determinations of species mixing ratios on Uranus and Neptune.

When planning future Ice Giant missions, investigators should keep in mind the key outstanding science questions related to atmospheric chemistry on Uranus and Neptune, and the ways in which these questions can be addressed:

- **What is the elemental composition of the deep atmospheres of Uranus and Neptune, and what does that tell us about planetary formation processes?** Determining the elemental composition of the deep atmosphere can help constrain the composition and properties of the gas and solid material accreted by the planet, helping to distinguish between competing theories of planetary formation and evolution [7]. Measurements of noble gases and their isotopes from *in situ* probes would be extremely valuable in this regard, as would obtaining vertical abundance profiles of CH<sub>4</sub>, NH<sub>3</sub>, H<sub>2</sub>S, and PH<sub>3</sub> down to tens of bars (and firm detections of NH<sub>3</sub> and PH<sub>3</sub> in the first place), and isotopic ratios of the main C, N, O carriers [7]. Measurements of the vertical profiles of disequilibrium quenched species such as CO, N<sub>2</sub>, and potentially CO<sub>2</sub> and PH<sub>3</sub> would also help constrain the deep oxygen and nitrogen abundance — a probe is unlikely to survive to deep enough pressures to measure the deep oxygen abundance on Uranus and Neptune. Microwave or radio observations from an orbiter or from the Earth can remotely sample deeper tropospheric levels, albeit with coarse vertical resolution and potential degeneracies in contributions from various opacity sources and temperatures, to help constrain the deep abundance of sulfur, nitrogen, and oxygen, as well as put any probe measurements in a more global 3D context.
- **How does the tropospheric composition vary in three dimensions across Uranus and Neptune, and what does that tell us about convection, circulation, and dynamics; what are the implications for determining deep elemental abundances?** Condensible tropospheric gases on the giant planets are observed to experience significant and unexpected variations in mixing ratio with latitude and altitude [28,33,34,117,118,122]. Determining how CH<sub>4</sub>, H<sub>2</sub>S, NH<sub>3</sub>, and H<sub>2</sub>O on Uranus and Neptune vary in a three-dimensional sense will help us better understand atmospheric circulation and convective processes in hydrogen-dominated atmospheres for which the condensate is heavier than the background gas (including on extrasolar planets). Determining the 3D distribution of disequilibrium quenched species such as CO, CO<sub>2</sub>, N<sub>2</sub>, and PH<sub>3</sub> would also shed light on convective processes in the deep troposphere where quenching occurs. Both remote sensing and *in situ* probe measurements can provide complementary information on tropospheric species distributions [106]. Probes can provide direct measurements of the thermal structure of a specific region or regions, which would provide an invaluable means with which contemporaneous remote-sensing observations can be calibrated to help break degeneracies between temperatures and abundances. Spatially resolved remote-sensing observations from ground-based or space-based facilities can help identify dynamically favorable entry regions for potential *in situ* probes to maximize the likelihood of sampling the deep atmospheric abundances [124].
- **Can disequilibrium chemical tracers such as CO, CO<sub>2</sub>, H<sub>2</sub>CO, C<sub>2</sub>H<sub>6</sub>, N<sub>2</sub>, HCN, and PH<sub>3</sub> provide robust indirect indicators of the deep abundance of O, N, P, and other elements?** Theoretical models suggest that these and other quenched disequilibrium species will have their mixing ratios frozen in when the rate of atmospheric transport exceeds that of key kinetic reactions in the deep troposphere; consequently, the observed upper tropospheric abundance can provide an indirect measure of the deep elemental abundances on Uranus and Neptune [17,29,39,40,51,97,106]. However, uncertainties in these models need to be reduced before we can make meaningful constraints on deep elemental abundances through this process (see section 3a). Moreover, the vertical profiles

and latitude distribution of these species would need to be obtained and combined with models to accurately determine the effect of external material and potentially latitude-dependent deep convection. Both *in situ* probes and remote-sensing observations would be useful in this regard, as would better constraints on vertical temperature profiles across the planet. If a probe is used to determine disequilibrium constituent abundances, having some means to distinguish between CO and N<sub>2</sub> — both with mass 28 amu, and both expected to be present in similar abundance — would be valuable, as could be obtained with a high-resolution mass spectrometer or specific targeted instrumentation.

- **How does the stratospheric composition vary in three dimensions across Uranus and Neptune, and what does that distribution tell us about atmospheric circulation, moist convection, atmospheric structure, chemical processes, response to seasonal forcing, and sources of external material?** The 3D distribution of stratospheric species depends on the source and distribution of the parent molecules, photochemical kinetics, seasonal variations in solar insolation, atmospheric transport, and aerosol microphysical processes. Identifying how constituents are distributed across the planet would help quantify the relative importance of the different processes. Spatially resolved mid-infrared spectroscopy from large ground-based telescope facilities can provide a means for mapping temperatures and photochemical-product abundances; however, such instrumentation on an Ice-Giant orbiter would provide better spatial resolution and coverage, particularly of winter hemispheres inaccessible from Earth. Temperature measurements from *in situ* probes would provide a valuable benchmark to calibrate such remote-sensing observations. Ultraviolet and near-infrared stellar and solar occultations could help identify new species and define how the methane homopause level varies across the planet, which in turn is important for understanding photochemical processes and coupled atmospheric dynamics and chemistry. Ground-based sub-millimeter observations can be used to monitor the distribution of CO, HCN, and CS to help identify the external sources and measure stratospheric winds. Sub-millimeter instruments on an Ice Giant orbiter could additionally provide measurements of H<sub>2</sub>O and perhaps H<sub>2</sub>CO, CH<sub>3</sub>OH, and CH<sub>3</sub>C<sub>2</sub>H. Ultraviolet, visible, and near-infrared observations at a variety of phase angles can help constrain the aerosol structure and scattering properties, which in turn can help characterize the distribution and composition of potential condensable gases. Mapping of stratospheric methane via near- and mid-infrared observations can further our understanding of how methane is transported past the tropopause cold trap into the stratospheres of Uranus and Neptune. Identifying how these processes work on our Ice Giants will help predict and understand exoplanet observations.
- **To what extent is cometary or other external debris affecting the troposphere, stratosphere, thermosphere, and ionosphere of Uranus and Neptune, and what are the implications for impact rates in the outer solar system, atmospheric structure and chemistry, and our ability to infer deep atmospheric abundances?** External material is clearly supplying the upper atmospheres of our Ice Giants with oxygen, nitrogen, and sulfur-bearing species and potentially other elements that would not normally be present in the upper atmosphere. This external material can strongly affect ionospheric chemistry and structure, stratospheric chemistry and aerosol formation, and radiative properties of the atmosphere. It is currently unclear whether this external material is contributing significantly to the CO abundance in the upper troposphere, which we need to resolve before we can use this potential quenched disequilibrium species as a tracer for the deep oxygen abundance on Uranus and Neptune. Obtaining accurate vertical profiles of CO in the lower stratosphere and upper troposphere from either *in situ* probes or remote-sensing observations that resolve line shapes will be critical for separating out the contributions from the internal and external sources of the CO. For similar reasons, as well as to identify the source of the external material, obtaining vertical profiles and

the spatial distribution of H<sub>2</sub>O, CO<sub>2</sub>, HCN, and CS would be valuable. In the near term, observations from ALMA and *JWST* can help provide some of this information.

- What is the composition and structure of the ionosphere of Uranus and Neptune, and what does that tell us about thermospheric processes, magnetospheric processes, and sources of external material?** We currently have very limited information about the ionospheric structure and composition on Uranus and Neptune. External material from the local satellite/ring systems, interplanetary dust particles, or cometary impacts can potentially affect the overall electron-density profile, chemical speciation, and layering within the ionosphere. The extent to which the Ice Giants' unusual offset, tilted, complex magnetic field influences ionospheric properties and promotes magnetosphere-atmosphere interactions is not well understood, nor is how the ionosphere varies spatially and temporally. Radio occultations from an Ice Giant orbiter would help map out ionospheric structure across the Ice Giants to help constrain ionospheric processes and the influence of external material. Near-infrared emission observations from an Ice Giant orbiter or Earth-based observations can monitor H<sub>3</sub><sup>+</sup> to track spatial and temporal variations in the ionosphere and help search for additional ionic species. Ultraviolet occultations could help map species such as benzene that are produced from ion-neutral chemistry and contribute to stratospheric haze deeper in the atmosphere.
- Why is the observable atmospheric composition of Uranus and Neptune so different, are these differences variable or static, and what are the implications for interior and deep atmospheric processes and atmospheric evolution? How is the atmospheric composition of Uranus and Neptune affected by the planet's internal heat flow, relative abundance of different elements, axial tilt, and orbital distance, and what are the implications for extrasolar planets?** Despite a similar mass, radius, and bulk composition, the observed atmospheric composition of Uranus and Neptune is very different. The two planets may have started out similarly but evolved differently, perhaps as a result of cataclysmic giant impacts [11–14]. Differences in internal heat flux between the two planets appear to lead to differences in the way the energy is transported through the atmosphere (e.g., [103]), which in turn leads to differences in atmospheric convection, tropospheric storm generation, and stratospheric mixing. Differences in planetary obliquity may also lead to differences in atmospheric chemistry and dynamics. To fully understand how different physical and chemical processes on the two planets have shaped their different atmospheric composition, and how that composition might be time-variable, we need the *in situ* probe and Ice Giant orbiter remote-sensing observations described above, along with monitoring of the composition over seasonal time scales from astronomical facilities on the ground and in space, and related accompanying laboratory and theoretical investigations into atmospheric properties and processes. Knowledge gained from studies of our Ice Giants should be considered from the more general context of how similar atmospheric chemical and physical processes apply to the diverse population of Neptune-class and sub-Neptune exoplanets within our galaxy.

Our mysterious Ice-Giant planets formed differently from both the Gas Giants and terrestrial planets; Uranus and Neptune are our only nearby representatives of a class of planet that is now known to be common in our galaxy. The atmospheric composition on Uranus and Neptune holds valuable clues to both solar-system formation processes and to physical and chemical processes that operate on intermediate-sized volatile-rich planets. To fully interpret these clues, we need to better understand the chemistry of these worlds and the complex coupling of chemistry, dynamics, and radiation that shape the observable atmospheric composition. Many of the key outstanding atmospheric chemistry questions discussed above cannot be answered through remote observations from the Earth, due to the vast distances involved and the restriction to the Earth-facing hemisphere — a dedicated exploration mission is required. The scientific motivation for a future Ice Giant mission has never been stronger, and these distant worlds are beckoning.

**Data Accessibility.** This article has no additional new data. The data presented in the figures can be obtained from the original journal and/or the authors of that originating article.

**Authors' Contributions.** J.M. led the project and wrote the paper. T.C., L.F., and M.R. provided comments, additions, and corrections to the paper.

**Competing Interests.** We declare no competing interests.

**Funding.** J.M. acknowledges support from the NASA Solar System Workings grant 80NSSC19K0536. T.C. acknowledges funding from CNES and from the Programme National de Planétologie (PNP) of CNRS/INSU. L.F. was supported by a Royal Society Research Fellowship at the University of Leicester. L.F. and M.R. acknowledge support from a European Research Council Consolidator Grant (under the European Union's Horizon 2020 research and innovation programme, grant agreement No. 723890).

**Acknowledgements.** We thank Emmanuel Lellouch and an anonymous reviewer for comments and suggestions that improved the manuscript.

## References

- Pollack JB, Hubickyj O, Bodenheimer P, Lissauer JJ, Podolak M, Greenzweig Y. 1996 Formation of the Giant Planets by Concurrent Accretion of Solids and Gas. *Icarus* **124**, 62–85.
- Helled R, Bodenheimer P. 2014 The formation of Uranus and Neptune: Challenges and implications for intermediate-mass exoplanets. *Astrophys. J.* **789**, 69.
- Helled R, Bodenheimer P, Podolak M, Boley A, Meru F, Nayakshin S, Fortney JJ, Mayer L, Alibert Y, Boss AP. 2014 Giant Planet Formation, Evolution, and Internal Structure. In Beuther H, Klessen RS, Dullemond CP, Henning T, editors, *Protostars and Planets VI* pp. 643–665 Tucson. Univ. Arizona Press.
- Batalha NM, Rowe JF, Bryson ST, Barclay T, Burke CJ, Caldwell DA, Christiansen JL, Mullally F, Thompson SE, Brown TM, Dupree AK, Fabrycky DC, Ford EB, Fortney JJ, Gilliland RL, Isaacson H, Latham DW, Marcy GW, Quinn SN, Ragozzine D, Shporer A, Borucki WJ, Ciardi DR, Gautier, III TN, Haas MR, Jenkins JM, Koch DG, Lissauer JJ, Rapin W, Basri GS, Boss AP, Buchhave LA, Carter JA, Charbonneau D, Christensen-Dalsgaard J, Clarke BD, Cochran WD, Demory BO, Desert JM, Devore E, Doyle LR, Esquerdo GA, Everett M, Fressin F, Geary JC, Girouard FR, Gould A, Hall JR, Holman MJ, Howard AW, Howell SB, Ibrahim KA, Kinemuchi K, Kjeldsen H, Klaus TC, Li J, Lucas PW, Meibom S, Morris RL, Prša A, Quintana E, Sanderfer DT, Sasselov D, Seader SE, Smith JC, Steffen JH, Still M, Stumpe MC, Tarter JC, Tenenbaum P, Torres G, Twicken JD, Uddin K, Van Cleve J, Walkowicz L, Welsh WF. 2013 Planetary Candidates Observed by Kepler. III. Analysis of the First 16 Months of Data. *Astrophys. J. Suppl. Ser.* **204**, 24.
- Fressin F, Torres G, Charbonneau D, Bryson ST, Christiansen J, Dressing CD, Jenkins JM, Walkowicz LM, Batalha NM. 2013 The False Positive Rate of Kepler and the Occurrence of Planets. *Astrophys. J.* **766**, 81.
- Petigura EA, Marcy GW, Howard AW. 2013 A Plateau in the Planet Population below Twice the Size of Earth. *Astrophys. J.* **770**, 69.
- Mousis O, Atkinson DH, Cavalié T, Fletcher LN, Amato MJ, Aslam S, Ferri F, Renard JB, Spilker T, Venkatapathy E, Wurz P, Aplin K, Coustenis A, Deleuil M, Dobrijevic M, Fouchet T, Guillot T, Hartogh P, Hewagama T, Hofstadter MD, Hue V, Hueso R, Lebreton JP, Lellouch E, Moses J, Orton GS, Pearl JC, Sánchez-Lavega A, Simon A, Venot O, Waite JH, Achterberg RK, Atreya S, Billebaud F, Blanc M, Borget F, Brugger B, Charnoz S, Chiavassa T, Cottini V, d'Hendecourt L, Danger G, Encrenaz T, Goriús NJP, Jorda L, Marty B, Moreno R, Morse A, Nixon C, Reh K, Ronnet T, Schmider FX, Sheridan S, Sotin C, Vernazza P, Villanueva GL. 2018 Scientific rationale for Uranus and Neptune in situ explorations. *Planet. Space Sci.* **155**, 12–40.
- Hofstadter M, Simon A, Atreya S, Banfield D, Fortney JJ, Hayes A, Hedman M, Hospodarsky G, Mandt K, Masters A, Showalter M, Soderlund KM, Turrini D, Turtle E, Reh K, Elliott J, Arora N, Petropoulos A, Ice Giant Mission Study Team. 2019 Uranus and Neptune missions: A study in advance of the next Planetary Science Decadal Survey. *Planet. Space Sci.* **177**, 104680.
- Mandt KE, Mousis O, Treat S. 2020 Determining the origin of the building blocks of the Ice

- Giants based on analogue measurements from comets. *Mon. Not. Roy. Astron. Soc.* **491**, 488–494.
10. Safronov VS. 1966 Sizes of the largest bodies falling onto the planets during their formation. *Sov. Astron.* **9**, 987–9916.
  11. Stevenson DJ. 1986 The Uranus-Neptune Dichotomy: the Role of Giant Impacts. *Lunar Planet. Sci. Conf.* **17**, 1011–1012.
  12. Podolak M, Helled R. 2012 What Do We Really Know about Uranus and Neptune?. *Astrophys. J. Lett.* **759**, L32.
  13. Kegerreis JA, Teodoro LFA, Eke VR, Massey RJ, Catling DC, Fryer CL, Korycansky DG, Warren MS, Zahnle KJ. 2018 Consequences of Giant Impacts on Early Uranus for Rotation, Internal Structure, Debris, and Atmospheric Erosion. *Astrophys. J.* **861**, 52.
  14. Reinhardt C, Chau A, Stadel J, Helled R. 2020 Bifurcation in the history of Uranus and Neptune: the role of giant impacts. *Mon. Not. Roy. Astron. Soc.* **492**, 5336–5353.
  15. Strobel DF, Yelle RV, Shemansky DE, Atreya SK. 1991 The upper atmosphere of Uranus. In Bergstralh JT, Miner ED, Matthews MS, editors, *Uranus* pp. 65–109 Tucson. Univ. Arizona Press.
  16. Atreya SK, Sandel BR, Romani PN. 1991 Photochemistry and vertical mixing. In Bergstralh JT, Miner ED, Matthews MS, editors, *Uranus* pp. 110–146 Tucson. Univ. Arizona Press.
  17. Fegley, B. J, Gautier D, Owen T, Prinn RG. 1991 Spectroscopy and chemistry of the atmosphere of Uranus. In Bergstralh JT, Miner ED, Matthews MS, editors, *Uranus* pp. 147–203 Tucson. Univ. Arizona Press.
  18. Bishop J, Atreya SK, Romani PN, Orton GS, Sandel BR, Yelle RV. 1995 The middle and upper atmosphere of Neptune. In Cruikshank DP, Matthews MS, Schumann AM, editors, *Neptune and Triton* pp. 427–487 Tucson. Univ. Arizona Press.
  19. Gautier D, Conrath BJ, Owen T, de Pater I, Atreya SK. 1995 The troposphere of Neptune. In Cruikshank DP, Matthews MS, Schumann AM, editors, *Neptune and Triton* pp. 547–611 Tucson. Univ. Arizona Press.
  20. Podolak M, Helled R, Schubert G. 2019 Effect of non-adiabatic thermal profiles on the inferred compositions of Uranus and Neptune. *Mon. Not. Roy. Astron. Soc.* **487**, 2653–2664.
  21. Moses JI, Fletcher LN, Greathouse TK, Orton GS, Hue V. 2018 Seasonal stratospheric photochemistry on Uranus and Neptune. *Icarus* **307**, 124–145.
  22. Hueso R, Sánchez-Lavega A. 2019 Atmospheric Dynamics and Vertical Structure of Uranus and Neptune's Weather Layers. *Space Sci. Rev.* **215**, 52.
  23. Gulkis S, Janssen MA, Olsen ET. 1978 Evidence for the depletion of ammonia in the Uranus atmosphere. *Icarus* **34**, 10–19.
  24. Briggs FH, Sackett PD. 1989 Radio observations of Saturn as a probe of its atmosphere and cloud structure. *Icarus* **80**, 77–103.
  25. de Pater I, Romani PN, Atreya SK. 1991 Possible microwave absorption by H<sub>2</sub>S gas in Uranus' and Neptune's atmospheres. *Icarus* **91**, 220–233.
  26. Irwin PGJ, Toledo D, Garland R, Teanby NA, Fletcher LN, Orton GA, Bézard B. 2018 Detection of hydrogen sulfide above the clouds in Uranus's atmosphere. *Nature Astronomy* **2**, 420–427.
  27. Irwin PGJ, Toledo D, Garland R, Teanby NA, Fletcher LN, Orton GS, Bézard B. 2019 Probable detection of hydrogen sulphide (H<sub>2</sub>S) in Neptune's atmosphere. *Icarus* **321**, 550–563.
  28. Tollefson J, de Pater I, Luszcz-Cook S, DeBoer D. 2019 Neptune's Latitudinal Variations as Viewed with ALMA. *Astron. J.* **157**, 251.
  29. Fegley, Jr. B, Prinn RG. 1985 Predicted chemistry of the deep atmosphere of Uranus before the Voyager 2 encounter. *Nature* **318**, 48–50.
  30. Fegley, Jr. B, Prinn RG. 1986 Chemical models of the deep atmosphere of Uranus. *Astrophys. J.* **307**, 852–865.
  31. Conrath B, Gautier D, Hanel R, Lindal G, Marten A. 1987 The helium abundance of Uranus from Voyager measurements. *J. Geophys. Res.* **92**, 15003–15010.
  32. Burgdorf M, Orton GS, Davis GR, Sidher SD, Feuchtgruber H, Griffin MJ, Swinyard BM. 2003 Neptune's far-infrared spectrum from the ISO long-wavelength and short-wavelength spectrometers. *Icarus* **164**, 244–253.
  33. Karkoschka E, Tomasko MG. 2009 The haze and methane distributions on Uranus from HST-STIS spectroscopy. *Icarus* **202**, 287–309.
  34. Karkoschka E, Tomasko MG. 2011 The haze and methane distributions on Neptune from HST-STIS spectroscopy. *Icarus* **211**, 780–797.

35. Irwin PGJ, Toledo D, Braude AS, Bacon R, Weilbacher PM, Teanby NA, Fletcher LN, Orton GS. 2019 Latitudinal variation in the abundance of methane ( $\text{CH}_4$ ) above the clouds in Neptune's atmosphere from VLT/MUSE Narrow Field Mode Observations. *Icarus* **331**, 69–82.
36. Stromovsky LA, Karkoschka E, Fry PM, Hammel HB, de Pater I, Rages K. 2014 Methane depletion in both polar regions of Uranus inferred from HST/STIS and Keck/NIRC2 observations. *Icarus* **238**, 137–155.
37. Hofstadter MD, Adumitroaie V, Butler BJ, Atreya SK. 2018 Microwave Sounding of Saturn and Uranus: Comparing Gas- and Ice-Giant Planets. *AGU Fall Meeting Abstracts* **2018**, P33E–3878.
38. DeBoer DR, Steffes PG. 1996 Estimates of the Tropospheric Vertical Structure of Neptune Based on Microwave Radiative Transfer Studies. *Icarus* **123**, 324–335.
39. Venot O, Cavalié T, Bounaceur R, Tremblin P, Brouillard L, Lhoussaine Ben Brahim R. 2020 New chemical scheme for giant planet thermochemistry. Update of the methanol chemistry and new reduced chemical scheme. *Astron. Astrophys.* **634**, A78.
40. Cavalié T, Venot O, Selsis F, Hersant F, Hartogh P, Leconte J. 2017 Thermochemistry and vertical mixing in the tropospheres of Uranus and Neptune: How convection inhibition can affect the derivation of deep oxygen abundances. *Icarus* **291**, 1–16.
41. Encrenaz T, Serabyn E, Weisstein EW. 1996 Millimeter spectroscopy of Uranus and Neptune: Constraints on CO and  $\text{PH}_3$  tropospheric abundances. *Icarus* **124**, 616–624.
42. Teanby NA, Irwin PGJ, Moses JI. 2019 Neptune's carbon monoxide profile and phosphine upper limits from Herschel/SPIRE: Implications for interior structure and formation. *Icarus* **775**, 86–98.
43. Orton GS, Fletcher LN, Moses JI, Mainzer AK, Hines D, Hammel HB, Martin-Torres FJ, Burgdorf M, Merlet C, Line MR. 2014 Mid-infrared spectroscopy of Uranus from the Spitzer Infrared Spectrometer: 1. Determination of the mean temperature structure of the upper troposphere and stratosphere. *Icarus* **243**, 494–513.
44. Lellouch E, Moreno R, Orton GS, Feuchtgruber H, Cavalié T, Moses JI, Hartogh P, Jarchow C, Sagawa H. 2015 New constraints on the  $\text{CH}_4$  vertical profile in Uranus and Neptune from Herschel observations. *Astron. Astrophys.* **579**, A121.
45. Orton GS, Moses JI, Fletcher LN, Mainzer AK, Hines D, Hammel HB, Martin-Torres J, Burgdorf M, Merlet C, Line MR. 2014 Mid-infrared spectroscopy of Uranus from the Spitzer infrared spectrometer: 2. Determination of the mean composition of the upper troposphere and stratosphere. *Icarus* **243**, 471–493.
46. Greathouse TK, Richter M, Lacy J, Moses J, Orton G, Encrenaz T, Hammel HB, Jaffe D. 2011 A spatially resolved high spectral resolution study of Neptune's stratosphere. *Icarus* **214**, 606–621.
47. Schulz B, Encrenaz T, Bézard B, Romani PN, Lellouch E, Atreya SK. 1999 Detection of  $\text{C}_2\text{H}_4$  in Neptune from ISO/PHT-S observations. *Astron. Astrophys.* **350**, L13–L17.
48. Fletcher LN, Drossart P, Burgdorf M, Orton GS, Encrenaz T. 2010 Neptune's atmospheric composition from AKARI infrared spectroscopy. *Astron. Astrophys.* **514**, A17.
49. Meadows VS, Orton G, Line M, Liang MC, Yung YL, van Cleve J, Burgdorf MJ. 2008 First Spitzer observations of Neptune: Detection of new hydrocarbons. *Icarus* **197**, 585–589.
50. Cavalié T, Moreno R, Lellouch E, Hartogh P, Venot O, Orton GS, Jarchow C, Encrenaz T, Selsis F, Hersant F, Fletcher LN. 2014 The first submillimeter observation of CO in the stratosphere of Uranus. *Astron. Astrophys.* **562**, A33.
51. Luszcz-Cook SH, de Pater I. 2013 Constraining the origins of Neptune's carbon monoxide abundance with CARMA millimeter-wave observations. *Icarus* **222**, 379–400.
52. Feuchtgruber H, Lellouch E, Encrenaz T, Bézard B, Coustenis A, Drossart P, Salama A, de Graauw T, Davis GR. 1999 Oxygen in the stratospheres of the giant planets and Titan. In Cox P, Kessler M, editors, *The Universe as Seen by ISO* vol. SP-427ESA Special Publication pp. 133–136.
53. Feuchtgruber H, Lellouch E, Orton G, de Graauw T, Vandenbussche B, Swinyard B, Moreno R, Jarchow C, Billebaud F, Cavalié T, Sidher S, Hartogh P. 2013 The D/H ratio in the atmospheres of Uranus and Neptune from Herschel-PACS observations. *Astron. Astrophys.* **551**, A126.
54. Rosenqvist J, Lellouch E, Romani PN, Paubert G, Encrenaz T. 1992 Millimeter-wave observations of Saturn, Uranus, and Neptune: CO and HCN on Neptune. *Astrophys. J. Letters* **392**, L99–L102.
55. Marten A, Gautier D, Owen T, Sanders DB, Matthews HE, Atreya SK, Tilanus RPJ, Deane JR. 1993 First observations of CO and HCN on Neptune and Uranus at millimeter wavelengths and the implications for atmospheric chemistry. *Astrophys. J.* **406**, 285–297.

56. Trafton LM, Geballe TR, Miller S, Tennyson J, Ballester GE. 1993 Detection of  $\text{H}_3^+$  from Uranus. *Astrophys. J.* **405**, 761.
57. Feuchtgruber H, Lellouch E, de Graauw T, Bézard B, Encrenaz T, Griffin M. 1997 External supply of oxygen to the atmospheres of the giant planets. *Nature* **389**, 159–162.
58. Bézard B, Romani PN, Feuchtgruber H, Encrenaz T. 1999 Detection of the methyl radical on Neptune. *Astrophys. J. Letters* **515**, 868–872.
59. Encrenaz T, Lellouch E, Drossart P, Feuchtgruber H, Orton GS, Atreya SK. 2004 First detection of CO in Uranus. *Astron. Astrophys.* **413**, L5–L9.
60. Burgdorf M, Orton G, van Cleve J, Meadows V, Houck J. 2006 Detection of new hydrocarbons in Uranus' atmosphere by infrared spectroscopy. *Icarus* **184**, 634–637.
61. Moreno R, Lellouch E, Cavalié T, Moullet A. 2017 Detection of CS in Neptune's atmosphere from ALMA observations. *Astron. Astrophys.* **608**, L5.
62. Guilloteau S, Dutrey A, Marten A, Gautier D. 1993 CO in the troposphere of Neptune: Detection of the  $J = 1-0$  line in absorption. *Astron. Astrophys.* **279**, 661–667.
63. Naylor DA, Davis GR, Griffin MJ, Clark TA, Gautier D, Marten A. 1994 Broad-band spectroscopic detection of the CO  $J=3-2$  tropospheric absorption in the atmosphere of Neptune. *Astron. Astrophys.* **291**, L51–L53.
64. Courtin R, Gautier D, Strobel D. 1996 The CO abundance on Neptune from HST observations. *Icarus* **123**, 37–55.
65. Lellouch E, Moreno R, Paubert G. 2005 A dual origin for Neptune's carbon monoxide?. *Astron. Astrophys.* **430**, L37–L40.
66. Marten A, Matthews HE, Owen T, Moreno R, Hidayat T, Biraud Y. 2005 Improved constraints on Neptune's atmosphere from submillimetre-wavelength observations. *Astron. Astrophys.* **429**, 1097–1105.
67. Hesman BE, Davis GR, Matthews HE, Orton GS. 2007 The abundance profile of CO in Neptune's atmosphere. *Icarus* **186**, 342–353.
68. Lellouch E, Hartogh P, Feuchtgruber H, Vandenbussche B, de Graauw T, Moreno R, Jarchow C, Cavalié T, Orton G, Banaszkiewicz M, Blecka MI, Bockelée-Morvan D, Crovisier J, Encrenaz T, Fulton T, Küppers M, Lara LM, Lis DC, Medvedev AS, Rengel M, Sagawa H, Swinyard B, Szutowicz S, Bensch F, Bergin E, Billebaud F, Biver N, Blake GA, Blommaert JADL, Cernicharo J, Courtin R, Davis GR, Decin L, Encrenaz P, Gonzalez A, Jehin E, Kidger M, Naylor D, Portyankina G, Schieder R, Sidher S, Thomas N, de Val-Borro M, Verdugo E, Waelkens C, Walker H, Aarts H, Comito C, Kawamura JH, Maestrini A, Peacocke T, Teipen R, Tils T, Wildeman K. 2010 First results of Herschel-PACS observations of Neptune. *Astron. Astrophys.* **518**, L152.
69. Irwin PGJ, Lellouch E, de Bergh C, Courtin R, Bézard B, Fletcher LN, Orton GS, Teanby NA, Calcutt SB, Tice D, Hurley J, Davis GR. 2014 Line-by-line analysis of Neptune's near-IR spectrum observed with Gemini/NIFS and VLT/CRIFES. *Icarus* **227**, 37–48.
70. Bishop J, Atreya SK, Romani PN, Sandel BR, Herbert F. 1992 Voyager 2 ultraviolet spectrometer solar occultations at Neptune: Constraints on the abundance of methane in the stratosphere. *J. Geophys. Res.* **97**, 11,681–11,694.
71. Orton GS, Lacy JH, Achtermann JM, Parmar P, Blass WE. 1992 Thermal spectroscopy of Neptune - The stratospheric temperature, hydrocarbon abundances, and isotopic ratios. *Icarus* **100**, 541–555.
72. Lellouch E, Romani PN, Rosenqvist J. 1994 The vertical Distribution and Origin of HCN in Neptune's Atmosphere. *Icarus* **108**, 112–136.
73. Encrenaz T, Feuchtgruber H, Atreya SK, Bézard B, Lellouch E, Bishop J, Edgington S, Degraauw T, Griffin M, Kessler MF. 1998 ISO observations of Uranus: The stratospheric distribution of  $\text{C}_2\text{H}_2$  and the eddy diffusion coefficient. *Astron. Astrophys.* **333**, L43–L46.
74. Bishop J, Romani PN, Atreya SK. 1998 Voyager 2 ultraviolet spectrometer solar occultations at Neptune: Photochemical modeling of the 125–165 nm lightcurves. *Planet. Space Sci.* **46**, 1–20.
75. Feuchtgruber H, Lellouch E, Bézard B, Encrenaz T, de Graauw T, Davis GR. 1999 Detection of HD in the atmospheres of Uranus and Neptune: a new determination of the D/H ratio. *Astron. Astrophys.* **341**, L17–L21.
76. Trafton LM, Miller S, Geballe TR, Tennyson J, Ballester GE. 1999  $\text{H}_2$  quadrupole and  $\text{H}_3^+$  emission from Uranus: The Uranian thermosphere, ionosphere, and aurora. *Astrophys. J.* **524**, 1059–1083.
77. Encrenaz T, Schulz B, Drossart P, Lellouch E, Feuchtgruber H, Atreya SK. 2000 The ISO spectra

- of Uranus and Neptune between 2.5 and 4.2  $\mu\text{m}$ : constraints on albedos and  $\text{H}_3^+$ . *Astron. Astrophys.* **358**, L83–L87.
78. Encrenaz T, Drossart P, Orton G, Feuchtgruber H, Lellouch E, Atreya SK. 2003 The rotational temperature and column density of  $\text{H}_3^+$  in Uranus. *Planet. Space Sci.* **51**, 1013–1016.
  79. Feuchtgruber H, Encrenaz T. 2003 The infrared spectrum of Neptune at 3.5–4.1 microns: Search for  $\text{H}_3^+$  and evidence for recent meteorological variations. *Astron. Astrophys.* **403**, L7–L10.
  80. Fouchet T, Lellouch E, Feuchtgruber H. 2003 The hydrogen ortho-to-para ratio in the stratospheres of the giant planets. *Icarus* **161**, 127–143.
  81. Hammel HB, Lynch DK, Russell RW, Sitko ML, Bernstein LS, Hewagama T. 2006 Mid-infrared ethane emission on Neptune and Uranus. *Astrophys. J. Letters* **644**, 1326–1333.
  82. Cavalié T, Billebaud F, Biver N, Dobrijevic M, Lellouch E, Brillet J, Lecacheux A, Hjalmarson Å, Sandqvist A, Frisk U, Olberg M, Bergin EA, Odin Team. 2008 Observation of water vapor in the stratosphere of Jupiter with the Odin space telescope. *Planet. Space Sci.* **56**, 1573–1584.
  83. Melin H, Stallard T, Miller S, Trafton LM, Encrenaz T, Geballe TR. 2011 Seasonal variability in the ionosphere of Uranus. *Astrophys. J.* **729**, 134.
  84. Irwin PGJ, de Bergh C, Courtin R, Bézard B, Teanby NA, Davis GR, Fletcher LN, Orton GS, Calcutt SB, Tice D, Hurley J. 2012 The application of new methane line absorption data to Gemini-N/NIFS and KPNO/FIS observations of Uranus' near-infrared spectrum. *Icarus* **220**, 369–382.
  85. Teanby NA, Irwin PGJ. 2013 An external origin for carbon monoxide on Uranus from Herschel/SPIRE?. *Astrophys. J. Lett.* **775**, L49.
  86. Fletcher LN, de Pater I, Orton GS, Hammel HB, Sitko ML, Irwin PGJ. 2014 Neptune at summer solstice: Zonal mean temperatures from ground-based observations, 2003–2007. *Icarus* **231**, 146–167.
  87. Rezac L, de Val-Borro M, Hartogh P, Cavalié T, Jarchow C, Rengel M, Dobrijevic M. 2014 New determination of the HCN profile in the stratosphere of Neptune from millimeter-wave spectroscopy. *Astron. Astrophys.* **563**, A4.
  88. Iino T, Mizuno A, Nakajima T, Hidemori T, Tsukagoshi T, Kato C. 2014 Search for sulfur-bearing species as remnant of cometary impact on Neptune. *Planet. Space Sci.* **104**, 211–215.
  89. Fletcher LN, Gustafsson M, Orton GS. 2018 Hydrogen Dimers in Giant-planet Infrared Spectra. *Astrophys. J. Suppl. Ser.* **235**, 24.
  90. Sromovsky LA, Karkoschka E, Fry PM, de Pater I, Hammel HB. 2019 The methane distribution and polar brightening on Uranus based on HST/STIS, Keck/NIRC2, and IRTF/SpEx observations through 2015. *Icarus* **317**, 266–306.
  91. Sromovsky LA, Fry PM, Kim JH. 2011 Methane on Uranus: The case for a compact  $\text{CH}_4$  cloud layer at low latitudes and a severe  $\text{CH}_4$  depletion at high-latitudes based on re-analysis of Voyager occultation measurements and STIS spectroscopy. *Icarus* **215**, 292–312.
  92. Luszcz-Cook SH, de Pater I, Wright M. 2013 Spatially-resolved millimeter-wavelength maps of Neptune. *Icarus* **226**, 437–454.
  93. Tice DS, Irwin PGJ, Fletcher LN, Teanby NA, Hurley J, Orton GS, Davis GR. 2013 Uranus' cloud particle properties and latitudinal methane variation from IRTF SpeX observations. *Icarus* **223**, 684–698.
  94. de Pater I, Fletcher LN, Luszcz-Cook S, DeBoer D, Butler B, Hammel HB, Sitko ML, Orton G, Marcus PS. 2014 Neptune's global circulation deduced from multi-wavelength observations. *Icarus* **237**, 211–238.
  95. Roman MT, Banfield D, Gierasch PJ. 2018 Aerosols and methane in the ice giant atmospheres inferred from spatially resolved, near-infrared spectra: I. Uranus, 2001–2007. *Icarus* **310**, 54–76.
  96. Roman MT, Fletcher LN, Orton GS, Rowe-Gurney N, Irwin PGJ. 2020 Uranus in northern midspring: Persistent atmospheric temperatures and circulations. *Astron. J.* **159**, 45.
  97. Prinn RG, Barshay SS. 1977 Carbon monoxide on Jupiter and implications for atmospheric convection. *Science* **198**, 1031–1034.
  98. Lodders K, Fegley, Jr. B. 1994 The origin of carbon monoxide in Neptunes's atmosphere. *Icarus* **112**, 368–375.
  99. Visscher C, Moses JI, Saslow SA. 2010b The deep water abundance on Jupiter: New constraints from thermochemical kinetics and diffusion modeling. *Icarus* **209**, 602–615.
  100. Moses JI, Visscher C, Fortney JJ, Showman AP, Lewis NK, Griffith CA, Klippenstein SJ, Shabram M, Friedson AJ, Marley MS, Freedman RS. 2011 Disequilibrium Carbon, Oxygen, and Nitrogen Chemistry in the Atmospheres of HD 189733b and HD 209458b. *Astrophys. J.* **737**, 15.

101. Visscher C, Moses JI. 2011 Quenching of Carbon Monoxide and Methane in the Atmospheres of Cool Brown Dwarfs and Hot Jupiters. *Astrophys. J.* **738**, 72.
102. Venot O, Hébrard E, Agúndez M, Dobrijevic M, Selsis F, Hersant F, Iro N, Bounaceur R. 2012 A chemical model for the atmosphere of hot Jupiters. *Astron. Astrophys.* **546**, A43.
103. Vazan A, Helled R. 2018 Explaining the low luminosity of Uranus: a self-consistent thermal and structural evolution. *Astron. Astrophys.* **610**, L14.
104. Leconte J, Selsis F, Hersant F, Guillot T. 2017 Condensation-inhibited convection in hydrogen-rich atmospheres. Stability against double-diffusive processes and thermal profiles for Jupiter, Saturn, Uranus, and Neptune. *Astron. Astrophys.* **598**, A98.
105. Moses JI, Visscher C, Keane TC, Sperier A. 2010 On the abundance of non-cometary HCN on Jupiter. *Faraday Discussions* **147**, 103–136.
106. Cavalié T, Venot O, Miguel Y, Fletcher LN, Wurz P, Mousis O, Bounaceur R, Hue V, Leconte J, Dobrijevic M. 2020 The deep composition of Uranus and Neptune from in situ exploration and thermochemical modeling. *Space Sci. Rev.* **216**, 58.
107. Gierasch PJ, Conrath BJ. 1985 Energy conversion processes in the outer planets. In Hunt GE, editor, *Recent Advances in Planetary Meteorology* pp. 121–146 Cambridge, UK. Cambridge University Press.
108. Wang D, Gierasch PJ, Lunine JI, Mousis O. 2015 New insights on Jupiter's deep water abundance from disequilibrium species. *Icarus* **250**, 154–164.
109. Moses JI. 2014 Chemical Kinetics on Extrasolar Planets. *Phil. Trans. R. Soc. A* **372**, 20130073.
110. Wang D, Lunine JI, Mousis O. 2016 Modeling the disequilibrium species for Jupiter and Saturn: Implications for Juno and Saturn entry probe. *Icarus* **276**, 21–38.
111. Visscher C, Fegley, Jr. B. 2005 Chemical Constraints on the Water and Total Oxygen Abundances in the Deep Atmosphere of Saturn. *Astrophys. J.* **623**, 1221–1227.
112. Kaye JA, Strobel DF. 1984 Phosphine photochemistry in the atmosphere of Saturn. *Icarus* **59**, 314–335.
113. Moses JI, Fouchet T, Yelle RV, Friedson AJ, Orton GS, Bézard B, Drossart P, Gladstone GR, Kostiuik T, Livengood TA. 2004 The stratosphere of Jupiter. In Bagenal F, Dowling TE, McKinnon WB, editors, *Jupiter. The Planet, Satellites and Magnetosphere* pp. 129–157 Cambridge. Cambridge Univ. Press.
114. Fouchet T, Moses JI, Conrath BJ. 2009 Saturn: Composition and Chemistry. In Dougherty MK, Esposito LW, Krimigis SM, editors, *Saturn from Cassini-Huygens* pp. 83–112. Springer.
115. Fletcher LN, Baines KH, Momary TW, Showman AP, Irwin PGJ, Orton GS, Roos-Serote M, Merlet C. 2011 Saturn's tropospheric composition and clouds from Cassini/VIMS 4.6–5.1  $\mu\text{m}$  nightside spectroscopy. *Icarus* **214**, 510–533.
116. Janssen MA, Ingersoll AP, Allison MD, Gulkis S, Laraia AL, Baines KH, Edgington SG, Anderson YZ, Kelleher K, Oyafuso FA. 2013 Saturn's thermal emission at 2.2-cm wavelength as imaged by the Cassini RADAR radiometer. *Icarus* **226**, 522–535.
117. Bolton SJ, Adriani A, Adumitroaie V, Allison M, Anderson J, Atreya S, Bloxham J, Brown S, Connerney JEP, DeJong E, Folkner W, Gautier D, Grassi D, Gulkis S, Guillot T, Hansen C, Hubbard WB, Iess L, Ingersoll A, Janssen M, Jorgensen J, Kaspi Y, Levin SM, Li C, Lunine J, Miguel Y, Mura A, Orton G, Owen T, Ravine M, Smith E, Steffes P, Stone E, Stevenson D, Thorne R, Waite J, Durante D, Ebert RW, Greathouse TK, Hue V, Parisi M, Szalay JR, Wilson R. 2017 Jupiter's interior and deep atmosphere: The initial pole-to-pole passes with the Juno spacecraft. *Science* **356**, 821–825.
118. Li C, Ingersoll A, Janssen M, Levin S, Bolton S, Adumitroaie V, Allison M, Arballo J, Bellotti A, Brown S, Ewald S, Jewell L, Misra S, Orton G, Oyafuso F, Steffes P, Williamson R. 2017 The distribution of ammonia on Jupiter from a preliminary inversion of Juno microwave radiometer data. *Geophys. Res. Lett.* **44**, 5317–5325.
119. Giles RS, Fletcher LN, Irwin PGJ, Orton GS, Sinclair JA. 2017 Ammonia in Jupiter's troposphere from high-resolution 5  $\mu\text{m}$  spectroscopy. *Geophys. Res. Lett.* **44**, 10,838–10,844.
120. Blain D, Fouchet T, Greathouse T, Encrenaz T, Charnay B, Bézard B, Li C, Lellouch E, Orton G, Fletcher LN, Drossart P. 2018 Mapping of Jupiter's tropospheric  $\text{NH}_3$  abundance using ground-based IRTF/TEXES observations at 5  $\mu\text{m}$ . *Icarus* **314**, 106–120.
121. de Pater I, Sault RJ, Wong MH, Fletcher LN, DeBoer D, Butler B. 2019 Jupiter's ammonia distribution derived from VLA maps at 3–37 GHz. *Icarus* **322**, 168–191.
122. Li C, Ingersoll A, Bolton S, Levin S, Janssen M, Atreya S, Lunine J, Steffes P, Brown S, Guillot T, Allison M, Arballo J, Bellotti A, Adumitroaie V, Gulkis S, Hodges A, Li L, Misra S, Orton

- G, Oyafuso F, Santos-Costa D, Waite H, Zhang Z. 2020 The water abundance in Jupiter's equatorial zone. *Nature Astronomy* **in press**.
123. Fletcher LN, Kaspi Y, Guillot T, Showman AP. 2020a How well do we understand the belt/zone circulation of Giant Planet atmospheres?. *Space Sci. Rev.* **216**, 30.
  124. Fletcher LN, de Pater I, Orton GS, Hofstadter MD, Irwin PGJ, Roman M, Toledo D. 2020b Ice giant circulation patterns: Implications for atmospheric probes. *Space Sci. Rev.* **216**, 21.
  125. Guillot T. 2019 Uranus and Neptune are key to understand planets with hydrogen atmospheres. *arXiv e-prints* p. arXiv:1908.02092.
  126. Stoker CR. 1986 Moist convection: A mechanism for producing the vertical structure of the Jovian Equatorial Plumes. *Icarus* **67**, 106–125.
  127. Lunine JI, Hunten DM. 1989 Abundance of condensable species at planetary cold traps: The role of moist convection. *Planet. Space Sci.* **37**, 151–166.
  128. Smith MD, Gierasch PJ. 1995 Convection in the outer planet atmospheres including ortho-para hydrogen conversion. *Icarus* **116**, 159–179.
  129. Stoker CR, Toon OB. 1989 Moist convection on Neptune. *Geophys. Res. Lett.* **16**, 929–932.
  130. Gierasch PJ, Ingersoll AP, Banfield D, Ewald SP, Helfenstein P, Simon-Miller A, Vasavada A, Breneman HH, Senske DA, Galileo Imaging Team. 2000 Observation of moist convection in Jupiter's atmosphere. *Nature* **403**, 628–630.
  131. Sugiyama K, Nakajima K, Odaka M, Kuramoto K, Hayashi YY. 2014 Numerical simulations of Jupiter's moist convection layer: Structure and dynamics in statistically steady states. *Icarus* **229**, 71–91.
  132. Ingersoll AP, Adumitroaie V, Allison MD, Atreya S, Bellotti AA, Bolton SJ, Brown ST, Gulkis S, Janssen MA, Levin SM, Li C, Li L, Lunine JI, Orton GS, Oyafuso FA, Steffes PG. 2017 Implications of the ammonia distribution on Jupiter from 1 to 100 bars as measured by the Juno microwave radiometer. *Geophys. Res. Lett.* **44**, 7676–7685.
  133. Mousis O, Atkinson DH, Ambrosi R, Atreya S, Banfield D, Barabash S, Blanc M, Cavalié T, Coustenis A, Deleuil M, Durré G, Ferri F, Fletcher L, Fouchet T, Guillot T, Hartogh P, Hueso R, Hofstadter M, Lebreton JP, Mandt KE, Rauer H, Rannou P, Renard JB, Sanchez-Lávega A, Sayanagi K, Simon A, Spilker T, Venkatapathy E, Waite JH, Wurz P. 2019 In situ Exploration of the Giant Planets. *arXiv e-prints* p. arXiv:1908.00917.
  134. Yelle RV, Doose LR, Tomasko MG, Strobel DF. 1987 Analysis of Raman scattered LY- $\alpha$  emissions from the atmosphere of Uranus. *J. Geophys. Res.* **14**, 483–486.
  135. Herbert F, Sandel BR, Yelle RV, Holberg JB, Broadfoot AL, Shemansky DE, Atreya SK, Romani PN. 1987 The upper atmosphere of Uranus: EUV occultations observed by Voyager 2. *J. Geophys. Res.* **92**, 15093–15109.
  136. Broadfoot AL, Atreya SK, Bertaux JL, Blamont JE, Dessler AJ, Donahue TM, Forrester WT, Hall DT, Herbert F, Holberg JB, Hunten DM, Krasnopolsky VA, Linick S, Lunine JI, McConnell JC, Moos HW, Sandel BR, Schneider NM, Shemansky DE, Smith GR, Strobel DF, Yelle RV. 1989 Ultraviolet spectrometer observations of Neptune and Triton. *Science* **246**, 1459–1466.
  137. Atreya SK, Ponthieu JJ. 1983 Photolysis of methane and the ionosphere of Uranus. *Planet. Space Sci.* **31**, 939–944.
  138. Romani PN, Atreya SK. 1988 Methane photochemistry and methane production on Neptune. *Icarus* **74**, 424–445.
  139. Romani PN, Atreya SK. 1989 Stratospheric aerosols from CH<sub>4</sub> photochemistry on Neptune. *Geophys. Res. Lett.* **16**, 941–944.
  140. Summers ME, Strobel DF. 1989 Photochemistry of the atmosphere of Uranus. *Astrophys. J.* **346**, 495–508.
  141. Bishop J, Atreya SK, Herbert F, Romani P. 1990 Reanalysis of Voyager 2 UVS occultations at Uranus: Hydrocarbon mixing ratios in the equatorial stratosphere. *Icarus* **88**, 448–464.
  142. Moses JI, Allen M, Yung YL. 1992 Hydrocarbon nucleation and aerosol formation in Neptune's atmosphere. *Icarus* **99**, 318–346.
  143. Romani PN, Bishop J, Bezard B, Atreya S. 1993 Methane photochemistry on Neptune: Ethane and acetylene mixing ratios and haze production. *Icarus* **106**, 442–463.
  144. Moses JI, Rages K, Pollack JB. 1995 An analysis of Neptune's stratospheric haze using high-phase-angle Voyager images. *Icarus* **113**, 232–266.
  145. Dobrijevic M, Parisot JP. 1998 Effect of chemical kinetics uncertainties on hydrocarbon production in the stratosphere of Neptune. *Planet. Space Sci.* **46**, 491–505.
  146. Moses JI, Fouchet T, Bézard B, Gladstone GR, Lellouch E, Feuchtgruber H. 2005

- Photochemistry and diffusion in Jupiter's stratosphere: Constraints from ISO observations and comparisons with other giant planets. *J. Geophys. Res.* **110**, E08001.
147. Dobrijevic M, Cavalié T, Hébrard E, Billebaud F, Hersant F, Selsis F. 2010 Key reactions in the photochemistry of hydrocarbons in Neptune's stratosphere. *Planet. Space Sci.* **58**, 1555–1566.
  148. Moses JI, Poppe AR. 2017 Dust ablation on the giant planets: Consequences for stratospheric photochemistry. *Icarus* **297**, 33–58.
  149. Lara LM, Rodrigo R, Moreno R, Lampón M. 2019 Analysis of the origin of water, carbon monoxide, and carbon dioxide in the Uranus atmosphere. *Astron. Astrophys.* **621**, A219.
  150. Dobrijevic M, Loison JC, Hue V, Cavalié T, Hickson KM. 2020 1D photochemical model of the ionosphere and the stratosphere of Neptune. *Icarus* **335**, 113375.
  151. Pollack JB, Rages K, Pope SK, Tomasko MG, Romani PN. 1987 Nature of the stratospheric haze on Uranus: Evidence for condensed hydrocarbons. *J. Geophys. Res.* **92**, 15037–15065.
  152. Pryor WR, West RA, Simmons KE, Delitsky M. 1992 High-phase-angle observations of Neptune at 2650 and 7500 Å: Haze structure and particle properties. *Icarus* **99**, 302–317.
  153. Hue V, Hersant F, Cavalié T, Dobrijevic M, Sinclair JA. 2018 Photochemistry, mixing and transport in Jupiter's stratosphere constrained by Cassini. *Icarus* **307**, 106–123.
  154. Greathouse TK, Lacy JH, Bézard B, Moses JI, Griffith CA, Richter MJ. 2005 Meridional variations of temperature, C<sub>2</sub>H<sub>2</sub> and C<sub>2</sub>H<sub>6</sub> abundances in Saturn's stratosphere at southern summer solstice. *Icarus* **177**, 18–31.
  155. Moses JI, Greathouse TK. 2005 Latitudinal and seasonal models of stratospheric photochemistry on Saturn: Comparison with infrared data from IRTF/TEXES. *J. Geophys. Res.* **110**, E09007.
  156. Howett CJA, Irwin PGJ, Teanby N, Simon-Miller A, Calcutt SB, Fletcher LN, de Kok R. 2007 Meridional Variations in Stratospheric Acetylene and Ethane in the Saturnian Atmosphere as Determined from Cassini/CIRS Measurements. *Icarus* **190**, 556–572.
  157. Fouchet T, Guerlet S, Strobel DF, Simon-Miller AA, Bézard B, Flasar FM. 2008 An equatorial oscillation in Saturn's middle atmosphere. *Nature* **453**, 200–202.
  158. Hesman BE, Jennings DE, Sada PV, Bjoraker GL, Achterberg RK, Simon-Miller AA, Anderson CM, Boyle RJ, Nixon CA, Fletcher LN, McCabe GH. 2009 Saturn's latitudinal C<sub>2</sub>H<sub>2</sub> and C<sub>2</sub>H<sub>6</sub> abundance profiles from Cassini/CIRS and ground-based observations. *Icarus* **202**, 249–259.
  159. Guerlet S, Fouchet T, Bézard B, Simon-Miller AA, Flasar FM. 2009 Vertical and meridional distribution of ethane, acetylene and propane in Saturn's stratosphere from CIRS/Cassini limb observations. *Icarus* **203**, 214–232.
  160. Guerlet S, Fouchet T, Bézard B, Moses JI, Fletcher LN, Simon-Miller AA, Flasar FM. 2010 Meridional distribution of CH<sub>3</sub>C<sub>2</sub>H and C<sub>4</sub>H<sub>2</sub> in Saturn's stratosphere from CIRS/Cassini limb and nadir observations. *Icarus* **209**, 682–695.
  161. Fletcher LN, Irwin PGJ, Teanby NA, Orton GS, Parrish PD, de Kok R, Howett C, Calcutt SB, Bowles N, Taylor FW. 2007 Characterising Saturn's vertical temperature structure from Cassini/CIRS. *Icarus* **189**, 457–478.
  162. Fletcher LN, Irwin PGJ, Orton GS, Teanby NA, Achterberg RK, Bjoraker GL, Read PL, Simon-Miller AA, Howett C, de Kok R, Bowles N, Calcutt SB, Hesman B, Flasar FM. 2008 Temperature and composition of Saturn's polar hot spots and hexagon. *Science* **319**, 79–82.
  163. Fletcher LN, Orton GS, Yanamandra-Fisher P, Fisher BM, Parrish PD, Irwin PGJ. 2009 Retrievals of atmospheric variables on the gas giants from ground-based mid-infrared imaging. *Icarus* **200**, 154–175.
  164. Fletcher LN, Achterberg RK, Greathouse TK, Orton GS, Conrath BJ, Simon-Miller AA, Teanby N, Guerlet S, Irwin PGJ, Flasar FM. 2010 Seasonal change on Saturn from Cassini/CIRS observations, 2004–2009. *Icarus* **208**, 337–352.
  165. Fletcher LN, Hesman BE, Achterberg RK, Irwin PGJ, Bjoraker G, Gorius N, Hurley J, Sinclair J, Orton GS, Legarreta J, García-Melendo E, Sánchez-Lavega A, Read PL, Simon-Miller AA, Flasar FM. 2012 The origin and evolution of Saturn's 2011–2012 stratospheric vortex. *Icarus* **221**, 560–586.
  166. Fletcher LN, Irwin PGJ, Sinclair JA, Orton GS, Giles RS, Hurley J, Gorius N, Achterberg RK, Hesman BE, Bjoraker GL. 2015 Seasonal evolution of Saturn's polar temperatures and composition. *Icarus* **250**, 131–153.
  167. Sinclair JA, Irwin PGJ, Fletcher LN, Moses JI, Greathouse TK, Friedson AJ, Hesman B, Hurley J, Merlet C. 2013 Seasonal variations of temperature, acetylene and ethane in Saturn's atmosphere from 2005 to 2010, as observed by Cassini-CIRS. *Icarus* **225**, 257–271.

168. Sinclair JA, Irwin PGJ, Fletcher LN, Greathouse T, Guerlet S, Hurley J, Merlet C. 2014 From Voyager-IRIS to Cassini-CIRS: Interannual variability in Saturn's stratosphere?. *Icarus* **233**, 281–292.
169. Sylvestre M, Guerlet S, Fouchet T, Spiga A, Flasar FM, Hesman B, Bjoraker GL. 2015 Seasonal changes in Saturn's stratosphere inferred from Cassini/CIRS limb observations. *Icarus* **258**, 224–238.
170. Hue V, Cavalié T, Dobrijevic M, Hersant F, Greathouse TK. 2015 2D photochemical modeling of Saturn's stratosphere. Part I: Seasonal variation of atmospheric composition without meridional transport. *Icarus* **257**, 163–184.
171. Moses JI, Armstrong ES, Fletcher LN, Friedson AJ, Irwin PGJ, Sinclair JA, Hesman BE. 2015 Evolution of stratospheric chemistry in the Saturn storm beacon region. *Icarus* **261**, 149–168.
172. Norwood J, Moses J, Fletcher LN, Orton G, Irwin PGJ, Atreya S, Rages K, Cavalié T, Sánchez-Lavega A, Hueso R, Chanover N. 2016 Giant planet observations with the James Webb Space Telescope. *Publications of the Astronomical Society of Pacific* **128**, 018005.
173. Poppe AR. 2016 An improved model for interplanetary dust fluxes in the outer Solar System. *Icarus* **264**, 369–386.
174. Moses JI. 1992 Meteoroid ablation in Neptune's atmosphere. *Icarus* **99**, 368–383.
175. Zahnle K. 1996 Dynamics and chemistry of SL9 plumes. In Noll KS, Weaver HA, Feldman PD, editors, *IAU Colloq. 156: The Collision of Comet Shoemaker-Levy 9 and Jupiter* pp. 183–212 Cambridge. Cambridge Univ. Press.
176. Lellouch E. 1996 Chemistry induced by the impacts: Observations. In Noll KS, Weaver HA, Feldman PD, editors, *IAU Colloq. 156: The Collision of Comet Shoemaker-Levy 9 and Jupiter* pp. 213–242 Cambridge. Cambridge Univ. Press.
177. Moses JI. 1996 SL9 impact chemistry: Long-term photochemical evolution. In Noll KS, Weaver HA, Feldman PD, editors, *IAU Colloq. 156: The Collision of Comet Shoemaker-Levy 9 and Jupiter* pp. 243–268 Cambridge. Cambridge Univ. Press.
178. Boslough MB, Crawford DA, Trucano TG, Robinson AC. 1995 Numerical modeling of Shoemaker-Levy 9 impacts as a framework for interpreting observations. *Geophys. Res. Lett.* **22**, 1821–1824.
179. Harrington J, de Pater I, Brecht SH, Deming D, Meadows V, Zahnle K, Nicholson PD. 2004 Lessons from Shoemaker-Levy 9 about Jupiter and planetary impacts. In Bagenal F, Dowling TE, McKinnon WB, editors, *Jupiter. The Planet, Satellites and Magnetosphere* pp. 159–184 Cambridge. Cambridge Univ. Press.
180. Lellouch E, Bézard B, Moreno R, Bockelée-Morvan D, Colom P, Crovisier J, Festou M, Gautier D, Marten A, Paubert G. 1997 Carbon monoxide in Jupiter after the impact of comet Shoemaker-Levy 9. *Planet. Space Sci.* **45**, 1203–1212.
181. Lellouch E, Bézard B, Moses JI, Davis GR, Drossart P, Feuchtgruber H, Bergin EA, Moreno R, Encrenaz T. 2002 The Origin of Water Vapor and Carbon Dioxide in Jupiter's Stratosphere. *Icarus* **159**, 112–131.
182. Moreno R, Marten A, Matthews HE, Biraud Y. 2003 Long-term evolution of CO, CS and HCN in Jupiter after the impacts of comet Shoemaker-Levy 9. *Planet. Space Sci.* **51**, 591–611.
183. Moreno R, Marten A. 2006 Mass losses of CO, CS and HCN on Jupiter/SL9. *Bull. Amer. Astronom. Soc.* **38**, 497.
184. Griffith CA, Bézard B, Greathouse T, Lellouch E, Lacy J, Kelly D, Richter MJ. 2004 Meridional transport of HCN from SL9 impacts on Jupiter. *Icarus* **170**, 58–69.
185. Lellouch E, Bézard B, Strobel DF, Bjoraker GL, Flasar FM, Romani PN. 2006 On the HCN and CO<sub>2</sub> abundance and distribution in Jupiter's stratosphere. *Icarus* **184**, 478–497.
186. Iino T, Ohyama H, Hirahara Y, Takahashi T, Tsukagoshi T. 2016 Submillimeter observation of Jupiter's stratospheric composition: Detection of carbon monosulfide (J=7-6) 19 years after the cometary impact. *Astron. J.* **152**, 179.
187. Moses JI, Allen M, Gladstone GR. 1995a Post-SL9 sulfur photochemistry on Jupiter. *Geophys. Res. Lett.* **22**, 1597–1600.
188. Moses JI, Allen M, Gladstone GR. 1995b Nitrogen and oxygen photochemistry following SL9. *Geophys. Res. Lett.* **22**, 1601–1604.
189. Lellouch E, Paubert G, Moreno R, Festou MC, Bézard B, Bockelée-Morvan D, Colom P, Crovisier J, Encrenaz T, Gautier D, Marten A, Despois D, Strobel DF, Sievers A. 1995 Chemical and thermal response of Jupiter's atmosphere following the impact of comet Shoemaker-Levy 9. *Nature* **373**, 592–595.

190. Moses JI, Lellouch E, Bézard B, Gladstone GR, Feuchtgruber H, Allen M. 2000 Photochemistry of Saturn's Atmosphere. II. Effects of an Influx of External Oxygen. *Icarus* **145**, 166–202.
191. Lyons JR. 1995 Metal ions in the atmosphere of Neptune. *Science* **267**, 648–651.
192. Bézard B, Lellouch E, Strobel D, Maillard JP, Drossart P. 2002 Carbon monoxide on Jupiter: Evidence for both internal and external sources. *Icarus* **159**, 95–111.
193. Moore L, Melin H, O'Donoghue J, Stallard T, Moses J, Galand M, Miller S, Schmidt C. 2019 Modelling  $\text{H}_3^+$  in planetary atmospheres: effects of vertical gradients on observed quantities. *Phil. Trans. Roy. Soc. A* **in press**, arXiv:1904.04284.
194. Capone LA, Whitten RC, Prasad SS, Dubach J. 1977 The ionospheres of Saturn, Uranus, and Neptune. *Astrophys. J.* **215**, 977–983.
195. Atreya SK, Donahue TM. 1975a Ionospheric models of Saturn, Uranus, and Neptune. *Icarus* **24**, 358–362.
196. Atreya SK, Donahue TM. 1975b The role of hydrocarbons in the ionospheres of the outer planets. *Icarus* **25**, 335–338.
197. Chandler MO, Waite JH. 1986 The ionosphere of Uranus: A myriad of possibilities. *Geophys. Res. Lett.* **13**, 6–9.
198. Shinagawa H, Waite JH. 1989 The ionosphere of Neptune. *Geophys. Res. Lett.* **16**, 945–947.
199. Melin H, Fletcher LN, Stallard TS, Johnson RE, O'Donoghue J, Moore L, Donnelly PT. 2018 The quest for  $\text{H}_3^+$  at Neptune: deep burn observations with NASA IRTF iSHELL. *Mon. Not. Roy. Astron. Soc.* **474**, 3714–3719.
200. Moses JI, Bass SF. 2000 The effects of external material on the chemistry and structure of Saturn's ionosphere. *J. Geophys. Res.* **105**, 7013–7052.
201. Matcheva KI, Strobel DF, Flasar FM. 2001 Interaction of gravity waves with ionospheric plasma: Implications for Jupiter's ionosphere. *Icarus* **152**, 347–365.
202. Lam HA, Miller S, Joseph RD, Geballe TR, Trafton LM, Tennyson J, Ballester GE. 1997 Variation in the  $\text{H}_3^+$  emission of Uranus. *Astrophys. J. Lett.* **474**, L73–L76.
203. Melin H, Stallard T, Miller S, Lystrup MB, Trafton LM, Booth TC, Rivers C. 2011 New limits on  $\text{H}_3^+$  abundance on Neptune using Keck NIRSPEC. *Mon. Not. Roy. Astron. Soc.* **410**, 641–644.
204. Melin H, Stallard TS, Miller S, Geballe TR, Trafton LM, O'Donoghue J. 2013 Post-equinoctial observations of the ionosphere of Uranus. *Icarus* **223**, 741–748.
205. Koskinen TT, Moses JI, West RA, Guerlet S, Jouchoux A. 2016 The detection of benzene in Saturn's upper atmosphere. *Geophys. Res. Lett.* **43**, 7895–7901.
206. Guerlet S, Fouchet T, Vinatier S, Simon AA, Dartois E, Spiga A. 2015 Stratospheric benzene and hydrocarbon aerosols detected in Saturn's auroral regions. *Astron. Astrophys.* **580**, A89.